Science Paper

Calcite Dissolution-Reprecipitation Reactions Are a Key Control on the Sr/Ca, Mg/Ca and $\delta^{88/86}$Sr Compositions of Himalayan River Waters

Emily I. Stevenson[1,2], Kevin W. Burton[3], Ian J. Parkinson[4], Rachael H. James[5], Basak Kisakürek[6], Ed Tipper[1], Michael Bickle[1] [a]

[1] Department of Earth Sciences, University of Cambridge, [2] Section 3.3: Earth Surface Geochemistry, Helmholtz Centre Potsdam - GFZ German Research Centre for Geosciences, [3] Department of Earth Sciences, University of Durham, [4] School of Earth Sciences, University of Bristol, [5] School of Ocean and Earth Science, National Oceanography Centres Southampton, University of Southampton, [6] GEOMAR Helmholtz Centre for Ocean Research Kiel

American Journal of Science

Silicate weathering on the continents is thought to play a critical part in regulating global climate on geological time scales but determination of the magnitude of silicate weathering fluxes is frustrated by the complexity of the weathering processes. Here we present analyses of stable Sr-isotopic compositions ($\delta^{88/86}$Sr) in a suite of river waters and bedloads from the Himalayas in Nepal to establish the lithological controls on $\delta^{88/86}$Sr values and the secondary processes that impact carbonate weathering. A control on $\delta^{88/86}$Sr values is lithology with the rivers in carbonate-dominated catchments marginally lower (~ 0.07 ‰) than in silicate-dominated catchments. However, as for ^{87}Sr/^{86}Sr ratios, $\delta^{88/86}$Sr values of carbonates are altered by silicate-carbonate mineral exchange during metamorphism. The major potential secondary control on $\delta^{88/86}$Sr values in Himalayan catchments is precipitation of secondary calcite responsible for the marked elevation of Sr/Ca and Mg/Ca ratios in the waters. We re-evaluate the mechanisms for secondary calcite formation and conclude that a balanced solution and re-precipitation process, driven by the relative instability of the primary Mg-rich calcite, provides a better explanation for the elevated Sr/Ca ratios than simple precipitation from a highly over saturated solution. This solution-re-precipitation process is akin to that invoked to explain diagenesis of deep-sea sediments. The mechanism of secondary calcite formation impacts the distinction of cation inputs from carbonate and silicate minerals. The correlation between $\delta^{88/86}$Sr water-calcite fractionations, Sr/Ca partition coefficients and precipitation rates allows the calcite re-precipitation rates to be inferred from the covariation of water $\delta^{88/86}$Sr values and Sr/Ca ratios. These rates are very low ($<10^{-8}$ mol m^{-2} s^{-1}) but are consistent with those inferred from field estimates of the amount of calcite re-precipitated, the surface area of carbonate exposed to weathering and the calcite weathering flux. The low precipitation rates are also consistent with previously reported $\Delta^{44/40}$Ca isotope fractionations of ~ -0.2‰. The calcite reprecipitation rates are comparable to silicate weathering rates previously inferred from Li-isotopic compositions which is consistent with calcite re-precipitation taking place very close to equilibrium following the initial rapid saturation of the fluids by calcite.

1. INTRODUCTION

The processes which control global climate on long timescales play a critical role in the evolution of our planet, yet the feedbacks which have kept the surface of the Earth habitable are not well understood (e.g., Berner et al., 1983; Chamberlin, 1898; Coogan & Dosso, 2015; Sleep & Zahnle, 2001; Walker et al., 1981). The marked global cooling over the last 50 million years should provide an accessible record of the processes responsible and consequently much attention has been paid to the potential impact of the exhumation of the Himalayas cooling climate through the increased 'weatherability' of rapidly eroding crust (e.g., Kump et al., 2000; Ruddiman, 1997). However, the difficulties in deconvolving the dissolved chemical fluxes from the Himalayan-Tibetan orogen into components derived from silicate mineral weathering by carbonic acid (which impacts

[a] Corresponding author: mb72@cam.ac.uk

long-term climate), carbonate mineral weathering by carbonic acid (which is climate-neutral in the long term), and sulphuric acid weathering (which may release CO_2), frustrates attempts to evaluate the potential impact of the orogen on climate (e.g., Bickle et al., 2015; English et al., 2000; Galy & France-Lanord, 1999; Harris et al., 1998; Krishnaswami & Singh, 1998; Tipper, Bickle, et al., 2006; Torres et al., 2014).

The systematics of carbonate weathering in the Himalayas has attracted much attention. The hypothesis that Himalayan carbonate ^{87}Sr/^{86}Sr ratios were elevated by metamorphic exchange with old silicate minerals (e.g., Palmer & Edmond, 1992; Quade et al., 1997) was verified by Bickle et al. (2001). This contributes to the high ^{87}Sr/^{86}Sr ratios of the Himalayan riverine discharge which is thought largely responsible for the marked rise in seawater ^{87}Sr/^{86}Sr ratios over the last 40 Ma (e.g., Edmond, 1992; Galy et al., 1999; Palmer & Edmond, 1992; Richter et al., 1992). A second distinctive characteristic of Himalayan rivers is that their Sr/Ca and Mg/Ca ratios are elevated well above those of their source bedrocks. This is ascribed to precipitation of secondary calcite with low Sr/Ca and Mg/Ca ratios in the river catchments (e.g., Bickle et al., 2015; Chen et al., 2022; English et al., 2000; Galy et al., 1999; Jacobson et al., 2002; Li et al., 2023; Tipper, Galy, et al., 2006). The lack of alternative sources with high Sr/Ca and Mg/Ca ratios, the observation that many Himalayan rivers are saturated or super-saturated in calcite and the presence of travertines in Himalayan catchments are all consistent with this hypothesis (see discussion in Jacobson et al., 2002). The precipitation of secondary calcite impacts the calculation of the fractions of Sr, Ca and Mg derived from silicate and carbonate mineral weathering (e.g., Bickle et al., 2015; Galy et al., 1999; Jacobson et al., 2002; Krishnaswami & Singh, 1998; Singh et al., 1998).

In this paper we use the mass-dependent fractionation of the stable isotopes of strontium, ^{88}Sr and ^{86}Sr, reported as $\delta^{88/86}$Sr ($\delta^{88/86}$Sr = ((^{88}Sr/^{86}Sr)$_{SAMP}$/(^{88}Sr/^{86}Sr)$_{NBS987}$)-1)x1000) to investigate lithological control on the riverine $\delta^{88/86}$Sr ratios as well as carbonate weathering systematics along with previous analyses of Ca-isotopic compositions (Tipper et al., 2008; Tipper, Galy, et al., 2006) from the same regions. $\delta^{88/86}$Sr data are presented for waters and bedload from rivers draining carbonate-dominated, silicate-dominated and mixed catchments in the Nepalese Himalayas using samples previously analyzed for major and trace cations, anions, ^{87}Sr/^{86}Sr ratios and lithium isotopic ratios (Bickle et al., 2015; Kisakürek et al., 2005).

Stable Sr isotopic values have widely been used in the study of chemical weathering processes (e.g., Andrews et al., 2016; Andrews & Jacobson, 2018; Bouchez & von Blanckenburg, 2021; Bullen & Chadwick, 2016; Chao et al., 2015; Stevenson et al., 2016; Wei et al., 2013) (fig. 1). One of the key controls on natural waters was proposed to be the solution of different minerals with distinct $\delta^{88/86}$Sr values in variable proportions (Andrews & Jacobson, 2018; Chao et al., 2015). de Souza et al. (2010), Andrews et al. (2016) and Bouchez and von Blanckenburg (2021) suggested that biomass uptake might elevate dissolved $\delta^{88/86}$Sr values.

Wei et al. (2013) observed a large seasonal variation in the Xijiang river ($\delta^{88/86}$Sr from 0.66 ‰ to 0.15 ‰) with the shift to lower $\delta^{88/86}$Sr values explained as due to increased carbonate input, (see Wu et al., 2024 for a recent review).

Here we show that the $\delta^{88/86}$Sr values of waters from carbonate-rich catchments tend to be lower than those from silicate-dominated catchments. However, the loss of Ca to secondary calcite in Himalayan river waters may fractionate $\delta^{88/86}$Sr values. Calcite exhibits precipitation-rate dependent fractionation of ^{88}Sr/^{86}Sr ratios (AlKhatib & Eisenhauer, 2017; Böhm et al., 2012). Shalev et al. (2017) estimated that precipitation of secondary calcites elevated the mean $\delta^{88/86}$Sr of global rivers by ~ 0.1‰. Stevenson et al. (2016) suggested that preferential uptake of low $\delta^{88/86}$Sr by precipitation of Fe-oxyhydroxides and clay minerals elevated dissolved $\delta^{88/86}$Sr in glacial meltwaters. It is important to understand how isotopic fractionations associated with precipitation of secondary minerals alter $\delta^{88/86}$Sr values to interpret river water compositions. In this paper the correlation between the $\delta^{88/86}$Sr and Sr/Ca ratios in samples from a carbonate-dominated catchment is used to place constraints on the mechanisms of carbonate weathering in these Himalayan catchments as well as on the magnitudes and formation rates of the secondary calcite.

2. STUDY AREAS

A range of samples from large and small rivers (main stem and tributaries) were analyzed from sample suites collected in the Nepalese Himalaya (fig. 2). The water samples were collected by Kisakürek et al. (2005) and bed-load sediments by Tipper, Bickle et al. (2006), Tipper, Galy et al. (2006), Tipper et al. (2008), and Bickle et al. (2015). Samples are representative of both carbonate and silicate lithologies at high (2000 to 4000 m) and low (550 to 1300 m) altitudes (table 1) and were collected both before and in the late monsoon. The samples are from the three main lithotectonic units of the Himalayas, the Tibetan Sedimentary Series (TSS), the High Himalayan Crystalline Series (HHCS) and Lesser Himalayan Series (LHS).

2.1. Tibetan Sedimentary Series (TSS)

The tributaries of the upper Marsyandi and Modi Khola (fig. 2) drain Tibetan Sedimentary Series rocks outcropping at altitudes of 3000 to 6000 m on the southern margin of the Tibetan plateau. Erosion rates are ~ 1 mm/yr (Gabet et al., 2008; Godard et al., 2012), monsoonal precipitation < 0.5 m/yr (Burbank et al., 2003) and the area is sparsely vegetated. The TSS consists of limestones, impure limestones and siliclastic sedimentary rocks with pyritic black shales. Metamorphic grades are mainly sub-greenschist facies, but higher grade calc-silicates are exposed in the eastern part of the Marsyandi catchment adjacent to the South Tibetan Detachment Surface (Bordet et al., 1971; Schneider & Masch, 1993; Searle & Godin, 2003). Searle and Godin (2003) assign the calc-silicate unit to the High Himalayan Crystalline Series (fig. 2). No evaporites, in particular gypsum, have been reported in the Marsyandi basin (Bordet et al., 1975).
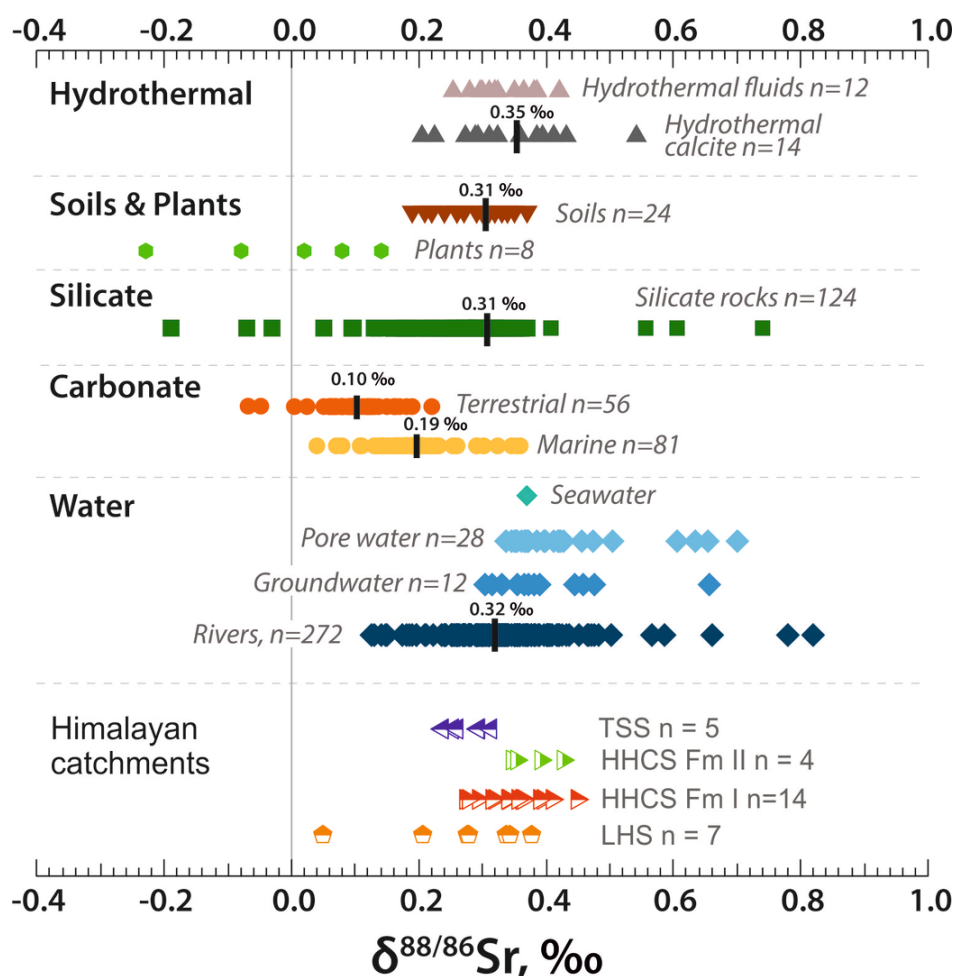
Figure 1. Ranges of published modern $\delta^{88/86}$Sr values (sources in Supplementary material, S1). Note the offset between terrestrial carbonates (carbonates precipitated on the continents) and river waters. Black lines are data means. Data from Himalayan catchments from this work (table 1).

2.2. The High Himalayan Crystalline Series (HHCS)

The High Himalayan Crystalline Series underlies the highest, partly glaciated, steepest and most rapidly eroding terrain with erosion rates ~ 3 mm/yr (West et al., 2015). The climate is Alpine with the monsoonal precipitation up to 4 m/yr. The samples were collected from tributaries of the Dudh Kosi, eastern Nepal, at altitudes of 2500 to 4000 m and from tributaries of the Indrawati, central Nepal, at altitudes of 800 to 1000 m where erosion rates are lower (~ 1 mm/yr, West et al., 2015) (fig. 1). Both catchments contain kyanite and some sillimanite-bearing metapelitic schists and gneisses (Formation I of Le Fort, 1975). In the Marsyandi catchment the two lowest samples from the Dudh Khola and Dana Khola (S22, S24) drain rocks from the High Himalayan Crystalline Series which here comprise calc-silicates containing diopside, amphibole, quartz and calcite bearing assemblages (Formation II), an augen gneiss unit (Formation III) and the Manaslu leucogranite (Le Fort, 1975).

2.3. Lesser Himalayan Series (LHS)

The Lesser Himalayan Series occupies terrain mainly below ~ 3000 m in altitude. The catchments are often densely forested with significant terracing for agriculture. Erosion rates are lower (~ 1 mm/yr, Godard et al., 2012; Vance et al., 2003) and precipitation ~ 2 m/yr. The samples are from tributaries of the Bhoti Kosi (fig. 1) where the LHS contains low grade abundant and often impure dolomites and limestones together with slates, quartzites and phyllites at altitudes of between 800 to 1300 m.

3. MATERIALS AND METHODS

The river waters above were sub-sampled from a suite of preserved (filtered and acidified to pH <2) water samples collected by Kisakürek et al. (2005) (see table S1 in supplementary information). Bedload samples from the Marsyandi River collected by Tipper, Bickle et al. (2006) and Bickle et al. (2015) were dried and powdered in a steel jaw crusher and an agate ball mill (Bickle et al., 2015). For the analyses of whole bed-load samples 10 mg was subject to hot plate dissolution using trace grade HF and HNO_3 acids (Stevenson et al., 2016).

The first batch of stable strontium isotope measurements (tables 1 & 2) was carried out on a Thermo-Finnigan Triton Thermal Ionisation Mass Spectrometer at the University of Durham as described by Stevenson et al. (2014).

**Table 1. Elemental and isotopic analyses of water**

Sample[b]	Lithology	Altitude m	Mg/Ca molar	Sr/Ca[a] nmol/μmol	$\delta^{88/86}$Sr	2se[c]	^{87}Sr/^{86}Sr	2se[d]	Bedload at same locality
Dudh Khosi (*) and tributaries									
A13*	FI HHCS	3909	0.092	0.785	0.342	0.012	0.726904	9	
A14	FI HHCS	3390	0.671	1.855	0.362	0.006	0.735069	10	
A15	FI HHCS	3050	0.116	0.834	0.365	0.014	0.740521	6	
A18	FI HHCS	2600	0.197	0.911	0.396	0.011	0.740455	9	
S1*	FI HHCS	2784	0.732	1.591	0.320	0.009	0.742036	16	
S3	FI HHCS	2876	0.116	0.772	0.449	0.008	0.739155	6	
S4	FI HHCS	2843	3.869	1.549	0.340	0.009	0.741630	9	
S5	FI HHCS	2567	0.202	0.908	0.410	0.011	0.741465	9	
Indrawati (**) and tributaries									
A10**	FI HHCS	848	0.139	1.414	0.390	0.013	0.734202	9	
A11	FI HHCS	800	0.379	1.841	0.274	0.008	0.740370	10	
A12	FI HHCS	800	0.317	1.970	0.294	0.008	0.737967	15	
S6**	FI HHCS	822	0.123	1.396	0.315	0.012	0.734735	6	
S7	FI HHCS	850	0.634	3.037	0.356	0.009	0.742816	9	
S8	FI HHCS	925	0.507	2.434	0.278	0.007	0.744484	11	
Tributaries of the Modi Khola									
A1	TSS	3590	0.276	1.707	0.314	0.030	0.733491	6	
A2	TSS	3082	0.178	2.976	0.347	0.006	0.717273	7	
A3	TSS FII HHCS	2540	0.042	0.916	0.354	0.011	0.716848	7	
Tributaries of the Marsyandi									
S17	TSS	3448	0.805	3.228	0.254	0.007	0.718708	6	BCT18
S18	TSS	3525	0.532	3.568	0.238	0.021	0.718554	7	BCT19
S19	TSS	3961	0.422	3.950	0.261	0.007	0.714545	8	ETT34 BCT23
S20	TSS	3210	0.485	1.671	0.295	0.007	0.725465	9	BCT29
S21	TSS	2900	0.217	2.080	0.294	0.007	0.714660	9	
S22	TSS FII HHCS	2359	0.056	0.944	0.427	0.016	0.724709	8	
S24	TSS FII HHCS	1999	0.057	0.948	0.392	0.011	0.721328	9	
Tributaries of the Bhote Kosi									
A6	LHS	972	0.697	0.267	0.378	0.015	0.846215	8	
A7	LHS	1225	0.734	0.552	0.338	0.014	0.836867	11	
A8	LHS	1283	0.796	0.363	0.207	0.009	0.836219	10	
A9	LHS	1060	0.848	0.259	0.050	0.018	0.818365	6	
S9	LHS	825	0.717	0.596	0.344	0.009	0.859081	9	
S10	LHS	1228	0.859	0.329	0.277	0.009	0.794646	9	
S12	LHS	966	0.644	0.305	0.279	0.013	0.863043	7	

[a] Data from Kisakürek et al. (2005)
[b] Sample number prefix 'S' collected in April/May 2002 and prefix 'A' collected October 2002. Locations given in table S1, supplementary information.
[c] internal precision. External precision estimated at ± 0.03 (2σ)
[d] Internal precision

Two aliquots of each sample (dissolved load or bedload) containing 500 ng of Sr were dried, re-dissolved in 1mL 2.0 M HNO_3 and one aliquot was spiked with an ^{87}Sr-^{84}Sr double spike (Pearce et al., 2015; Stevenson et al., 2014, 2016). The procedural Sr blank was less than ~ 30 pg, constituting less than 0.1 % of the total Sr analyzed. The isotope data were deconvolved from the spiked and un-spiked analyses using an exponential fractionation law and a New-
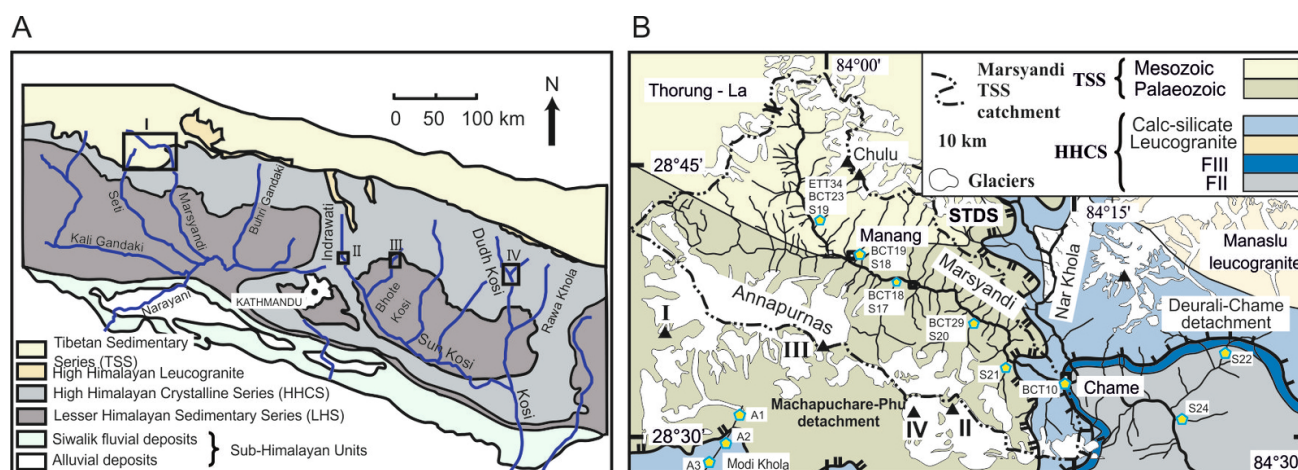
Figure 2. A) Geology and catchments sampled in the Nepalese Himalaya, modified after Kisakürek et al. (2005) and Parsons et al. (2016) with: I) Marsyandi and its tributaries; (II) Indrawati and its tributaries; (III) Bhoti Kosi and its tributaries; (IV) Dudh Kosi and its tributaries. Location of samples given in table S1 supplementary information. **B)** Geology and sample localities in the Marsyandi and Modi Khola catchments with the base of the TSS defined by the STDS and the Deurali-Chame detachment within the HHCS after Searle and Godin (2003). Bedload samples have prefix BCT or ETT and dissolved load samples have prefix S or A.

ton-Raphson iterative technique (Albarède & Beard, 2004). The internal precision on the ^{88}Sr/^{86}Sr isotope ratio varied between ± 7 to ± 15 ppm. The external reproducibility of SRM987 ^{87}Sr/^{86}Sr ratio normalised to ^{86}Sr/^{88}Sr = 0.1194 was 0.710226 ± 0.000006 (2σ, ± 8.4 ppm, n = 33). Repeat measurements of IAPSO seawater standard gave $\delta^{88/86}$Sr values of +0.38 ± 0.03‰ (2σ n = 8) identical to those of de Souza et al. (2010), Fietzke and Eisenhauer (2006), and Krabbenhöft et al. (2010). BCR-2 gave a $\delta^{88/86}$Sr value of +0.28 ± 0.05‰ (2σ, n=3), indistinguishable from the values of Ma et al. (2013) and Moynier et al. (2010).

The second batch of strontium isotope measurements on the bed load acetic acid leaches (table 2) was carried out on a Neptune Plus multicollector-ICP-mass spectrometer (Thermo Scientific) at the University of Cambridge. Samples and standards were doped with zirconium in the concentration ratio 2:1. Mass bias was estimated from the drift in the ^{92}Zr/^{90}Zr and ^{88}Sr/^{86}Sr ratios and corrected for using an exponential normalisation following Xu et al. (2020). The IAPSO seawater standard gave an ^{87}Sr/^{86}Sr ratio of 0.709200 ± 19 and an $\delta^{88/86}$Sr value of +0.389 ± 0.037‰ (2σ on 4 repeats) and Hastings seawater (a Cambridge internal seawater standard) an ^{87}Sr/^{86}Sr ratio of 0.709188 ± 26 and an $\delta^{88/86}$Sr value of +0.391 ± 0.027 ‰ (2σ on 9) (together, all the seawater values gave $\delta^{88/86}$Sr = 0.390 ± 0.029‰ (2σ, n= 13, our best estimate of external reproducibility, table S2 in supplementary information). Standard BHVO2 gave an ^{87}Sr/^{86}Sr ratio of 0.703500 ± 65, within error of 0.703479 ± 20 (Weis et al., 2006), and an $\delta^{88/86}$Sr value of 0.25 ± 0.055 ‰ (2se internal errors, n=1), within error of 0.267 ± 0.010 (Klaver et al., 2020). Sr/Ca ratios and Sr contents of the carbonate fraction of bedload samples (table 2) were measured by leaching in cold 10% acetic acid for 8 hours and analyzed by inductively coupled plasma optical emission spectroscopy using synthetic standards similar in composition to the leaches. Additional elements analyzed (Ca, K, Mg,

Na, Sr) are listed in table S3 in the supplementary information.

The water cation concentrations from Kisakürek et al. (2005) (table S1 Supplementary Information) are corrected for precipitation and hot spring inputs after Bickle et al. (2015). As noted previously by Bickle et al. (2015), corrections for Na are ~ 25% and the other major cations less than ~12%. For the Marsyandi, Modi Khola and Bhote Kosi catchments the fraction of Sr from precipitation and hot springs averages 3.4% (range 0 to 9%) and the impact on $\delta^{88/86}$Sr values is unlikely to be significant unless the hot springs have $\delta^{88/86}$Sr values well outside the range of any terrestrial samples. The water samples from the HHCS Formation I have lower Sr concentrations and higher Cl concentrations resulting in higher Sr fractions apparently derived from precipitation and hot springs (averaging 25% and in sample S4 estimated at greater than 100%). There is considerable scatter in both the available major ion analyses of Himalayan precipitation (Galy & France-Lanord, 1999) and the hot spring compositions (Becker et al., 2008; Evans et al., 2004). The larger corrections to Sr are therefore uncertain and $\delta^{88/86}$Sr ratios have not been analyzed in either the local precipitation or hot springs. The samples from the Dudh Kosi and Indrawati exhibit no significant correlation between $\delta^{88/86}$Sr values and the estimated fraction of Sr from precipitation and hot springs suggesting that rain and hot spring inputs have $\delta^{88/86}$Sr values within the range of the water samples.

4. RESULTS

4.1. Tibetan Sedimentary Series (TSS)

The TSS samples analyzed for $\delta^{88/86}$Sr were collected in the pre-monsoon from tributaries to Marsyandi between 3200 and 3950 m (samples S17 to S21) and post-monsoon from

Table 2. Isotopic analyses of bedloads and acetic acid leaches of bedloads

Sample[1]	Digest	Lithology	Sr/Ca	$\delta^{88/86}$Sr	2se[2]	^{87}Sr/^{86}Sr	2se	% carb Sr	Sr μmol /kg	°N	°E
BCT-10	Whole bed-load[3]	TSS	0.956	0.262	0.010	0.715483	30	60	3629	28.5524	84.2405
	Acetic leach[3]	TSS	0.687	0.260	0.019	0.713582	38		2134		
BCT-18	Whole bed-load[3]	TSS	0.948	0.259	0.016	0.713092	30	83	5094	28.6451	84.0699
	Acetic leach[4]	TSS		0.258	0.017	0.711636	39				
BCT-19	Whole bed-load[3]	TSS	2.036	0.223	0.011	0.719050	20	57	2476	28.6633	84.0279
	Acetic leach[4]	TSS	1.162	0.293	0.020	0.714537	22		1416		
BCT-21	Whole bed-load[3]	TSS	2.115	0.321	0.010	0.719936	70	26	2206	28.6693	84.0177
	Acetic leach[4]	TSS		0.318	0.011	0.714888	46				
BCT23	Whole bed-load[3]	TSS		0.219	0.013	0.712946	50	71		28.6996	83.9904
BCT29	Whole bed-load[3]	TSS	0.851	0.292	0.011	0.718952	30	87	3026	28.6108	84.1553
ETT34B	Whole bed-load[5]	TSS		0.352	0.012	0.712120	20	57	3447	28.6996	83.9906
	Acetic leach[4]	TSS	2.151	0.270	0.013	0.711291	21		1959		
BCT77b	Acetic leach[4]	LHS	0.176	0.343	0.016	0.751204	64		107	27.8419	85.8867
BCT81b	Acetic leach[4]	F1 HHCS	1.371	0.126	0.020	0.736691	47		50	27.8366	85.5770
GCR8b	Acetic leach[4]	Flood Plain	0.333	0.167	0.010	0.720808	69		1555		

[1] Bedloads from TSS outcrop drained by the Marsyandi except BCT77 from a tributary to the Bhote Kosi in the LHS catchment, and BCT81 from the HHCS in the Indrawati (cf. water sample A10). GCR8 was sampled from a carbonate nodule enclosing a root at a depth of ~ 2m in Siwalik sediments in the Ganges flood plain near Lucknow. [2] Internal precision. External precision is estimated at 0.03 2σ. [3] Sr/Ca ratios on whole rock samples from Bickle et al. (2015), $\delta^{88:86}$Sr analyses at Durham. [4] Sr/Ca ratios from this work, $\delta^{88:86}$Sr analyses at Cambridge. [5] Whole rock Sr concentration analysed by XRF as described in Bickle et al. (2015). $\delta^{88:86}$Sr analysis at Durham.

a tributary to the Modi Khola at 3560 m (sample A1). Previous work has shown that the ratio of carbonate to silicate inputs to the TSS Marsyandi catchment decreases during the dry season attributed to deeper groundwater flow paths (Tipper, Bickle, et al., 2006). The tributaries draining the TSS have ^{87}Sr/^{86}Sr between 0.7145 to 0.7335 and high concentrations of Sr (1000 to 6300 nmol/L) (table 1, fig. 3). The ^{87}Sr/^{86}Sr ratios are within the range reported for carbonates within the TSS (0.71 to 0.75, e.g., Bickle et al., 2015; Jacobson et al., 2002). Sr/Ca ratios (quoted as mmol/mol ratios) vary from 1.7 to 3.9. $\delta^{88/86}$Sr ranges from 0.238 to 0.295‰ in the Marsyandi and the one sample from a tributary to the Modhi Khola in the TSS has a $\delta^{88/86}$Sr of 0.314‰.

Bedloads from tributaries to the Marsyandi and one mainstem Marsyandi sample (BCT10, table 2) have whole bedload ^{87}Sr/^{86}Sr ratios between 0.712 and 0.720 and $\delta^{88/86}$Sr values between 0.219‰ and 0.352‰. Acetic acid leaches of TSS bedloads from the Marsyandi, which represent the calcite fraction, have $\delta^{88/86}$Sr values between 0.260 and 0.318‰. Bickle et al. (2015) report a more extensive set of acetic acid leaches of TSS bedloads and these have ^{87}Sr/^{86}Sr ratios between 0.711 and 0.7135, Sr contents between 2000 and 4000 mmol/kg, Ca contents between 3000 and 4000 mmol/kg, Sr/Ca ratios between 0.625 and 0.825 (mmol/mol) and Mg/Ca molar ratios between 0.042 to 0.52. Mg/Ca ratios of HCl leaches are similar consistent with observation that dolomite is absent from the Marsyandi TSS catchment.

4.2. The High Himalayan Crystalline Series (HHCS)

Streams draining two units of contrasting lithologies have been sampled in the HHCS. The Dudh Kola and the Indrawati catchments comprise typical HHCS lithologies of high and medium grade gneisses, migmatites and quartzites. Tributaries draining these units have intermediate ^{87}Sr/^{86}Sr ratios (0.7269 to 0.7445, Kisakürek et al., 2005, fig. 3) at the low end of the range for silicate rocks in the HHCS (0.73 to 0.90; e.g., Ahmad et al., 2000; Jacobson et al., 2002). Concentrations of Sr in streams that drain the HHCS range from 40 to 139 nmol/L in the Dudh Kosi at high altitudes (~2500 to 4000 m), to 118 to 455 nmol/L in Indrawati at lower altitudes (<1000m). Rain and hotspring corrected Sr/Ca values are also lower in the Dudh Kosi (~ 1.1) than the Indrawati (~2.1). $\delta^{88/86}$Sr in the Dudh Kosi ranges from 0.320 to 0.449‰ (mean 0.373, n=8). The Indrawati is slightly lower, ranging from 0.274 to 0.390‰ (mean 0.318‰, n=6). Samples from both rivers were taken in both pre- and post-monsoon but the average Sr-isotopic compositions in these different seasons exhibit no systematic differences (table 1). Samples A10 and S6 were collected from the mainstem Indrawati and have $\delta^{88/86}$Sr values in the same range as the Dudh Kosi, as does sample S7 from a small tributary in a predominantly gneissic unit. Samples A11 and S8 with a lower $\delta^{88/86}$Sr of 0.274‰ and 0.278 ‰ are from small streams which traverse a carbonate-bearing schist unit (Duvadi et al., 2005). The samples from the Annapurna region (S22 from the Dudh Khola and S24 from the Dana Khola which drain into the Marsyandi

and A2 and A3 from small tributaries to the Modi Khola), drain Formation II rocks which are high grade calc-silicate rocks whose assemblages include amphibole, diopside, scapolite and an average of ~ 27 volume % calcite (Becker, 2005). Their ^{87}Sr/^{86}Sr ratios (0.717 to 0.725, fig. 3) are significantly lower than those of the silicate dominated HHCS but their $\delta^{88/86}$Sr values (0.347 to 0.427‰) are similar to the other HHCS rivers. In the calc-silicates the Ca-Mg silicate minerals are primarily a product of dolomite breakdown reactions. Thus, the Sr-isotopic compositions of the carbonate and silicate minerals will have been brought to equilibrium during the Himalayan metamorphism.

The acetic acid leach of only one sample of HHCS bedload (sample BCT81 from the Indrawati) has been analyzed. This contains very little Sr (50 mmol/kg) with high Sr/Ca and Mg/Ca ratios, a high ^{87}Sr/^{86}Sr ratio (0.737) and a low $\delta^{88/86}$Sr value (0.126‰). The very low Sr content would make the leach composition sensitive to addition of components leached from silicate minerals as its relatively high Na/Ca ratio (51 mmol/mol) attests. The high Mg/Ca ratio (0.3) implies that the carbonate leached is 40% (mol fraction) dolomite.

4.3. Lesser Himalayan Series (LHS)

Waters from tributaries of the Bhoti Kosi draining the LHS have very radiogenic ^{87}Sr/^{86}Sr ratios (0.7947 to 0.8630) similar to the carbonate and silicate rocks from the LHS (e.g., Bickle et al., 2001; Oliver et al., 2003) and intermediate levels of Sr (150 to 334 nmol/L). Sr/Ca ratios of 0.27 to 0.60 are low (table 1, fig. 3). The $\delta^{88/86}$Sr values of the waters span a wide range from 0.050 to 0.378‰, and there are no detectable differences between samples taken pre- and post-monsoon. The acetic acid leach of LHS bedload sample BCT77 from a small tributary to the Bhote Kosi contains little Sr (107 mmol/kg) and has a high Mg/Ca ratio (0.77) implying that most of the leached carbonate is dolomite. This sample has an ^{87}Sr/^{86}Sr ratio of 0.751 and a $\delta^{88/86}$Sr value of 0.345‰, the high $\delta^{88/86}$Sr value being consistent with exchange with silicate minerals, characteristic of LHS carbonates (e.g., Bickle et al., 2001). The wide range of the $\delta^{88/86}$Sr values of the LHS samples is intriguing but more data are needed on the bedrock samples to interpret the data.

5. DISCUSSION

5.1. Lithological control

A key control on the water $\delta^{88/86}$Sr values appears to be lithology with rivers draining carbonate-dominated catchments (e.g., the TSS) exhibiting lower $\delta^{88/86}$Sr values than those draining silicates (e.g., the HHCS, figs. 3, 4, table 1), as expected from the global compilation of rock $\delta^{88/86}$Sr values (fig. 1). Thus, rivers draining the silicate-dominated HHCS formation I in the Dudh Kosi catchment tributaries have a mean $\delta^{88/86}$Sr value of 0.373 ± 0.030‰ (2se, n=8), and in the Indrawati catchment 0.318 ± 0.038‰ (n=6). The carbonate-dominated TSS catchments in the Marsyandi have a mean $\delta^{88/86}$Sr value of 0.268 ± 0.022‰ (n=5). A small tributary to the Modi Khola in the TSS has a $\delta^{88/}$
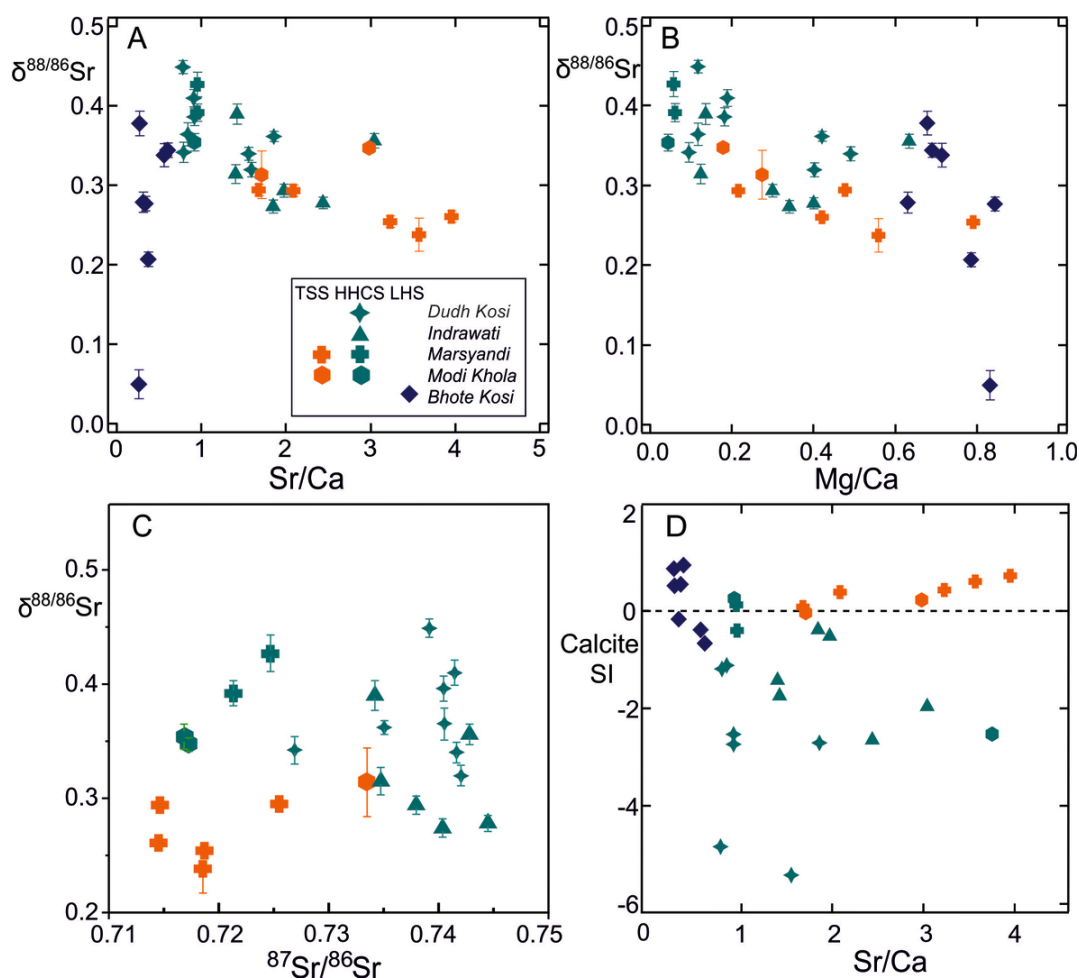
Figure 3. A), B) and C) **δ$^{88/86}$Sr values plotted against Sr/Ca, Mg/Ca and ^{87}Sr/^{86}Sr for water samples ([table 1](#)) corrected for cyclic and hot spring inputs as in Bickle et al. (2015). Higher Sr/Ca and Mg/Ca ratios associated with lower δ$^{88/86}$Sr values in the carbonate-rich TSS catchments interpreted to result from precipitation of secondary calcite. D) Calcite saturation index, SI, calculated using PHREEQC v3 with the PHREEQC database (sample analyses, pH and temperature given in [table 1](#) and table S1 supplementary information), versus Sr/Ca.**

^{86}Sr value of 0.314‰. The mean δ$^{88/86}$Sr value of the Dudh Kosi and Indrawati silicate catchment tributaries (0.349 ± 0.027‰, 2se n=14) is significantly higher than the mean of the TSS carbonate-dominated tributaries (0.276 ± 0.024‰, n=7) with the probability of the two distributions being indistinguishable ~0.001 (Welch's t-test).

## 5.2. Sr-isotope exchange between silicate and carbonate minerals

The δ$^{88/86}$Sr analyses of acetic acid leaches of four samples of the Marsyandi bedloads overlap at the 2σ level and have a mean value of 0.270 ± 0.032 ‰ (2σ), a scatter comparable with the estimated external reproducibility of the analyses ([table 2](#)). The fifth sample, BCT21, has a higher δ$^{88/86}$Sr value (0.318) and higher ^{87}Sr/^{86}Sr ratio (0.7149) ([fig. 5A](#)). This shift in both the radiogenic and stable Sr-isotopic composition of BCT21 carbonate, the sample with the smallest fraction of carbonate Sr ([table 2](#)), is consistent with the observation that Himalayan metamorphism has caused Sr-exchange between silicate and carbonate minerals (e.g., Bickle et al., 2001) with the silicates characterised

by higher ^{87}Sr/^{86}Sr and δ$^{88/86}$Sr ratios. The much greater abundance of carbonates in the TSS catchment is reflected in their lower ^{87}Sr/^{86}Sr and δ$^{88/86}$Sr ratios than the HHCS samples.

Three of the five acetic acid leaches (BCT10, BCT18 & BCT21) have δ$^{88/86}$Sr values within error of the whole bedload values although the ^{87}Sr/^{86}Sr ratios of the whole bedload and acetic acid leaches of these samples differ significantly, reflecting the much larger signal-to-precision ratio of the ^{87}Sr/^{86}Sr system ([fig. 5B & C](#)). It should be noted that even if carbonates exchange Sr with silicate minerals, this takes place over length scales of less than a metre (Bickle et al., 2001). Therefore, the bulk carbonate and silicate fractions in bedload derived from lithologically diverse catchments would not necessarily exhibit apparent equilibrium in Sr-isotopic compositions even if equilibrium was attained within individual lithological units.

Two of the bedload samples were collected from the same small stream in 2002 pre- and post-monsoon (BCT23 and ETT34B) and their whole bed-load δ$^{88/86}$Sr values are distinct well outside of uncertainty (0.22‰ vs 0.35‰). It is likely that the bedload of the smaller tributaries are not
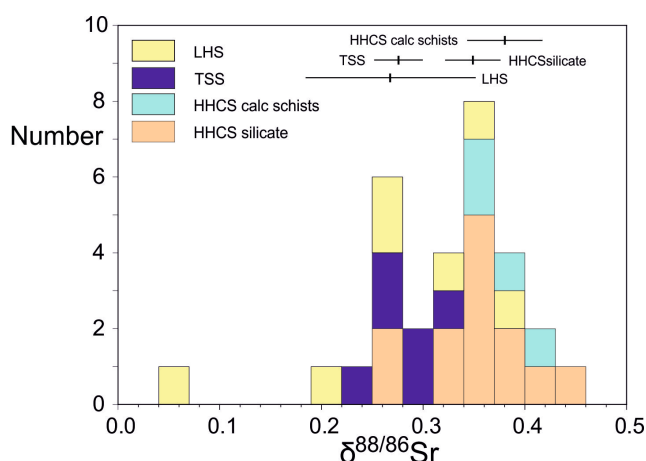
Figure 4. Histogram of $\delta^{88/86}$Sr values classified by litho-tectonic unit. Carbonate-bearing units from HHCS (Formation II in the Annapurna region and calc-schist containing units in Indrawati catchment) distinguished. Means and 2 x standard error uncertainties of means are shown for the major litho-tectonic units.

well mixed and reflect individual landslide events (e.g., Niemi et al., 2005). This may also explain why the $\delta^{88/86}$Sr value of the acetic leach from BCT19 (0.29) is much higher than the whole bed-load sample (0.22 ‰) and the water sample (S18, 0.238 ‰).

The best estimate of the mean carbonate $\delta^{88/86}$Sr value in the Marsyandi is from the acetic acid leach of sample BCT10 (0.260) which represents an average of the whole Marsyandi TSS catchment. This is higher than the average present-day marine carbonate (0.19 ‰, fig.1) and the flux-weighted mean $\delta^{88/86}$Sr value of Sr exported from the oceans of 0.21 ± 0.02 (2σ) (Krabbenhöft et al., 2010). This is just within error of the average $\delta^{88/86}$Sr value of deep ocean carbonate oozes of 0.23 ± 0.02 (2σ) analyzed by Voigt et al. (2015). As discussed above, the carbonate $\delta^{88/86}$Sr values in the Marsyandi bedload are likely elevated from the original sedimentary (post-diagenetic) composition of the source limestones by exchange with silicate Sr during the Himalayan metamorphism. This is reflected by their ^{87}Sr/^{86}Sr ratios (0.711 to 0.714) which are well above pristine marine carbonate values (0.707 to 0.709). Elevation of the ^{87}Sr/^{86}Sr ratio of the carbonate fraction of BCT10 from a likely marine value of ~ 0.708 would require that ~ 20% of its Sr was derived from silicate with a ^{87}Sr/^{86}Sr ratio of 0.731, that of the silicate residue from leaching (Bickle et al., 2015). If the original silicate had a $\delta^{88/86}$Sr value of ~ 0.35‰, the mean of silicate catchments sampled here, subtraction of 20% of silicate Sr implies that the pre-Himalayan metamorphism carbonate $\delta^{88/86}$Sr value would have been 0.23‰.

5.3. Secondary weathering processes: precipitation of calcite

The similarity between the estimates of the $\delta^{88/86}$Sr values of the carbonate inputs to the Marsyandi waters (0.26‰)

and the carbonate source bed-loads (0.27‰) is perhaps surprising given that previous work has argued that between 65 and 80% of the dissolved Ca has been precipitated as secondary calcites (Bickle et al., 2015). The magnitude of stable-Sr-isotopic fractionation between fluid and calcite (~ -0.05 to -0.30 ‰, e.g., Böhm et al., 2012) implies that the fluid $\delta^{88/86}$Sr values may be fractionated by precipitation of the secondary calcites. We examine models for secondary calcite precipitation and Sr-isotopic fractionation to reconcile this observation and constrain the kinetics of the processes.

The elevation of Sr/Ca and Mg/Ca ratios by precipitation of secondary calcite in Himalayan rivers has previously been modelled by Rayleigh fractionation from a starting solution with Sr/Ca and Mg/Ca ratios of the source carbonate (e.g., Bickle et al., 2015; Galy et al., 1999; Jacobson et al., 2002). In this model the inferred maximum loss of 70 to 80% Ca from the waters implies very high starting Ca concentrations (e.g., Ca ~ 5000 mol/L in the Marsyandi time series samples collected near Chame; Tipper, Galy, et al., 2006). A similar high Ca starting composition was inferred for rivers and springs in the Jura Mountains if their elevated Sr/Ca ratios reflected Rayleigh fractionation (Calmels, 2007). Such high Ca concentrations, charge balanced by HCO_3^- are implausible unless the carbonate system in the river is far from equilibrium with the atmosphere. They are also significantly higher than the maximum concentrations of ~ 3500 µmol/L seen in a global dataset of carbonate-draining river compositions compiled by Gaillardet et al. (2019), higher than any tributaries and cold springs in the Marsyandi catchment (maximum 1825 µmol/L Ca) and only surpassed by hot springs. However, the latter have significant inputs of CO_2 derived from metamorphic decarbonation reactions (Becker et al., 2008), are confined to the Marsyandi mainstem valley bottom and make negligible contributions to the tributaries in which the $\delta^{88/86}$Sr ratios reported here were measured (Evans et al., 2004).

An alternative mechanism to explain the high Sr/Ca and Mg/Ca ratios in river waters suggested by Calmels (2007) is that the calcite re-crystallises by a solution-exchange process so that the water Ca concentrations may be maintained near a constant concentration. Such a process is used to explain the diagenetic alteration of seafloor sediments where the biogenic high-Mg calcites are unstable with respect to low-Mg calcite and the recrystallisation drives Sr and Mg return fluxes to the ocean (Gieskes et al., 1975; Richter & DePaolo, 1987). The key observation that Gieskes and Kastner (1975) made to justify the assumption of recrystallisation of the original high Sr-carbonate to a low Sr-carbonate was that the fluid showed a much larger increase in Sr than Ca concentrations. The waters in the Marsyandi show comparable trends with a negligible change in Ca concentration with Sr/Ca ratio whereas Sr concentration increases by a factor of ~ 9 (fig. 6). These trends do not represent mixing with inputs from silicate weathering as these are small based on analyses of silicate fractions of Marsyandi bedloads (Bickle et al., 2015).
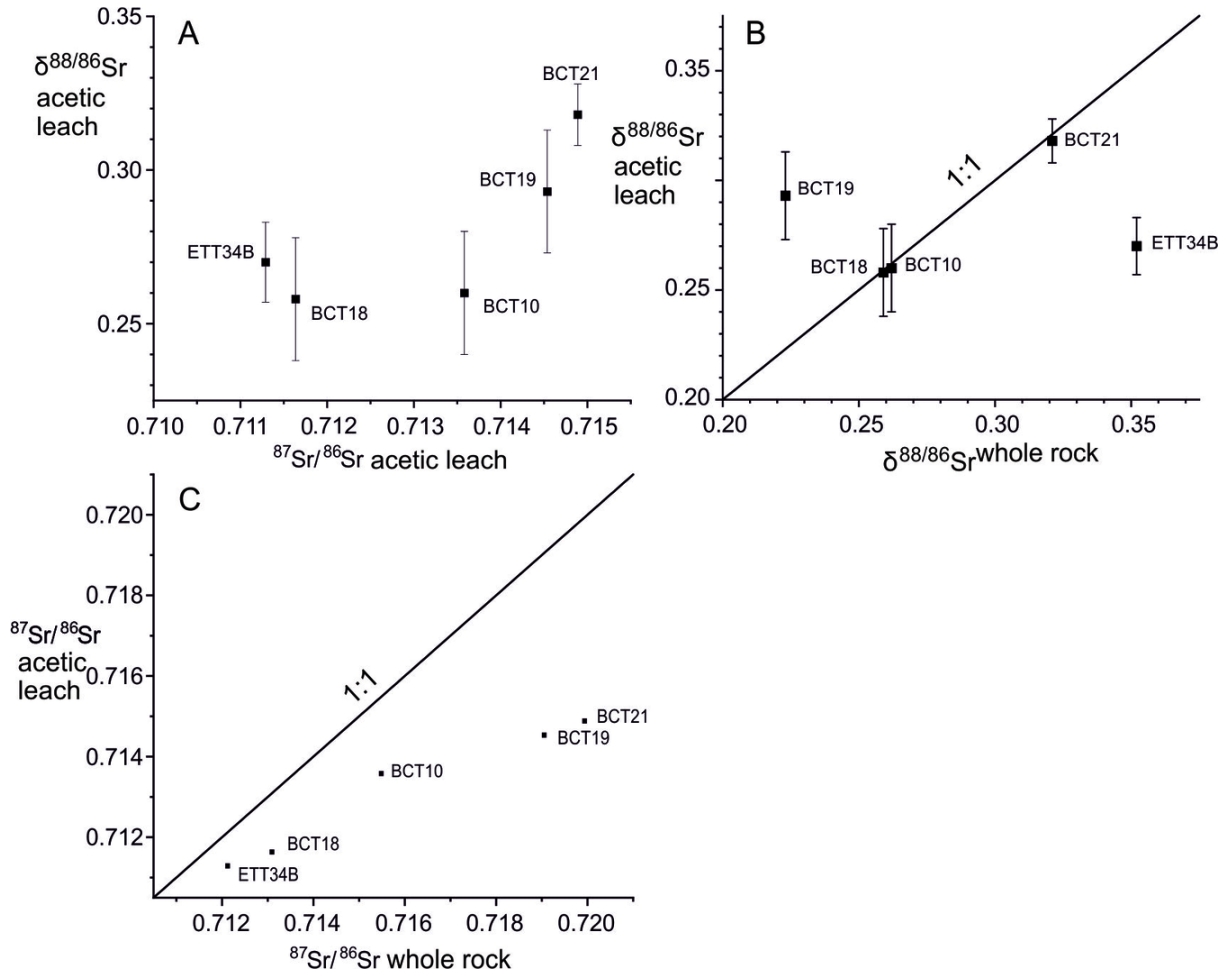
Figure 5. Sr isotopic compositions of TSS Marsyandi bed load samples. Error bars 2σ A) $\delta^{88/86}$Sr plotted against ^{87}Sr/^{86}Sr ratios for bedload acetic acid leaches. B) $\delta^{88/86}$Sr of acetic acid leaches plotted against $\delta^{88/86}$Sr of whole bed-load analyses. C) ^{87}Sr/^{86}Sr ratios of acetic acid leaches plotted against ^{87}Sr/^{86}Sr ratios of whole bed-load analyses. 2σ uncertainties (table 2) smaller than symbols.

We therefore evaluate a solution-repreciptation model to explain the elevated Sr/Ca in Himalayan waters and calculate how Sr and Ca concentrations and stable Sr and Ca isotopic ratios might be expected to vary with Sr/Ca ratios as a function of re-precipitation rate.

6. MODELS FOR PRECIPITATION OF SECONDARY CALCITE

6.1. Fractionation factors for water-calcite $\delta^{88/86}$Sr values

The fractionation factors between water and calcite stable Sr- and Ca-isotopic ratios ($\Delta^{88/86}$Sr, $\Delta^{44/40}$Ca) are inversely related to the Sr/Ca partition coefficient ($K_D^{Sr/Ca}$) (fig. 7A), defined as,

$$K_D^{Sr/Ca} = \frac{Sr/Ca|_{calcite}}{Sr/Ca|_{water}} \qquad (1)$$

The Sr/Ca partition coefficient and isotopic fractionation factors are functions of fluid chemistry and temperature and precipitation rate (fig. 7B). However, their covariation is, within the precision of the data, only dependent on precipitation rate (AlKhatib & Eisenhauer, 2017; Böhm et al., 2012; DePaolo, 2011; Gabitov et al., 2014; Z. Zhang & Wang, 2024). Models of the processes which control the Sr- and Ca-isotopic and Sr/Ca partition coefficient infer kinetic control by a surface reaction process although they differ on details of the process (e.g., DePaolo, 2011; Mills et al., 2021; Z. Zhang & Wang, 2024). Data from laboratory experiments and natural samples for water compositions with high Ca^{2+}: CO_3^{2-} ratios is consistent with the $\Delta^{88/86}$Sr and $\Delta^{44/40}$Ca isotopic fractionations being close to zero at equilibrium, that is at low reaction rates, and tending to a limit ($\Delta^{88/86}$Sr ~ -0.4‰, $\Delta^{44/40}$Ca ~ -2‰) at rapid reaction rates (Z. Zhang & Wang, 2024). Zhang and DePaulo (2021) infer that the equilibrium value of the Sr/Ca partition coefficient is ~ 0.025 from slowly precipitated marine calcites and Zhang and Wang (2024) estimate that $K_D^{Sr/Ca}$ = 0.24 at the kinetic limit. This allows the Sr and Ca isotope and elemental partitioning coefficients to be parameterised with relatively simple and self-consistent expressions against precipitation rate (Z. Zhang & Wang, 2024). The covariation of stable Sr- and Ca-isotopic ratios with Sr/Ca ratios can therefore be used to put further constraints on the rate and mechanisms of secondary calcite precipitation.
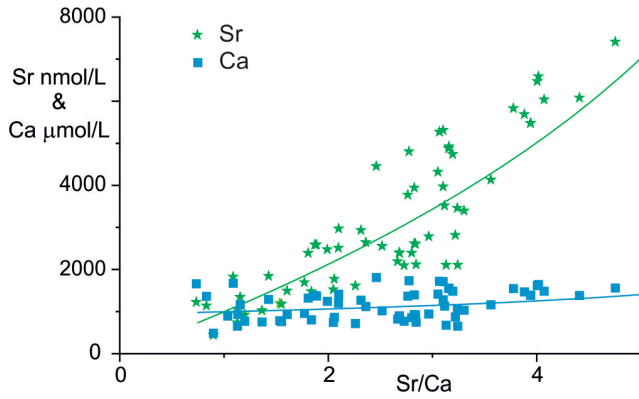
Figure 6. Variation of Ca and Sr against Ca/Sr ratio for the times series samples collected over two years at Chame in the mainstem Marsyandi close to where it leaves the TSS catchment (Tipper, Bickle et al., 2006). Lines denote the best fit for the evolution of Ca and Sr concentrations (eqs S18 and S23 in supplementary information) for a dissolution-reprecipitation model which gives ε= -0.04 ± 0.05 (1σ), where ε is the fractional difference in the rate of precipitation of secondary calcite to dissolution of primary calcite. Calculated given $K_D^{Sr/Ca}$ = 0.05, Sr_F^0 = 735 nmol/L and Ca_F^0 = 980 μmol/L. Ca and Sr are corrected by subtracting silicate inputs calculated using the Na/Ca and Sr/Ca ratios of the leached BCT10 bedload (Bickle et al., 2015).

6.2. Modeling calcite solution and re-precipitation

6.2.1. INTRODUCTION

We model the isotopic and elemental fractionations caused by the calcite solution and re-precipitation process by reactive transport along a one-dimensional flow path through a porous medium (cf. Fontorbe et al., 2013; Maher, 2010). We consider the evolution of a fluid flowing through a carbonate rock matrix in which the reactions with calcite dominate the water chemistry. Further, since the kinetics of calcite solution are rapid, we envisage that the fluid approaches calcite saturation near to the start of the flow path. In rapidly eroding Himalayan catchments where solution reactions are incomplete it may be assumed that the composition of the rock, reaction rates and isotopic fractionation factors remain constant with time and that the time-varying term in the differential equation is small (see discussion of the quasi-steady state assumption in Lichtner (1988) and discussion of the results of our modeling below). Therefore, the concentration of a component in the fluid (e.g., Ca_F) at any given distance, x, is assumed constant with time.

6.2.2. MATHEMATICAL MODELS

The equations describing the evolution of Ca, Sr and their isotopic ratios, making the stationary-state assumption (Lichtner, 1988), may be written as a function of the precipitation to dissolution rate (terms are defined in table S4 in supplementary information). The mass balance of Ca (mol m^{-3}) is given by

$$\omega_0 \phi \frac{\partial Ca_F}{\partial x} = R_{Ca} - R_{Ca}(1 + \epsilon) = -R_{Ca}\,\epsilon \qquad (2)$$

where R_{Ca} is the rate Ca is supplied by mineral dissolution (mol Ca m^{-3} s^{-1}) and 1+ ε describes the rate of precipitation of secondary calcite relative to the rate of supply by mineral dissolution. When ε= 0 re-precipitation balances dissolution, when ε = -1 re-precipitation is zero and when ε → ∞ the system tends to Rayleigh fractionation with dissolution negligible compared to precipitation.

Making the approximation that the range of isotopic compositions is small, the variation in Ca-isotopic values with reactive transport may then be described by
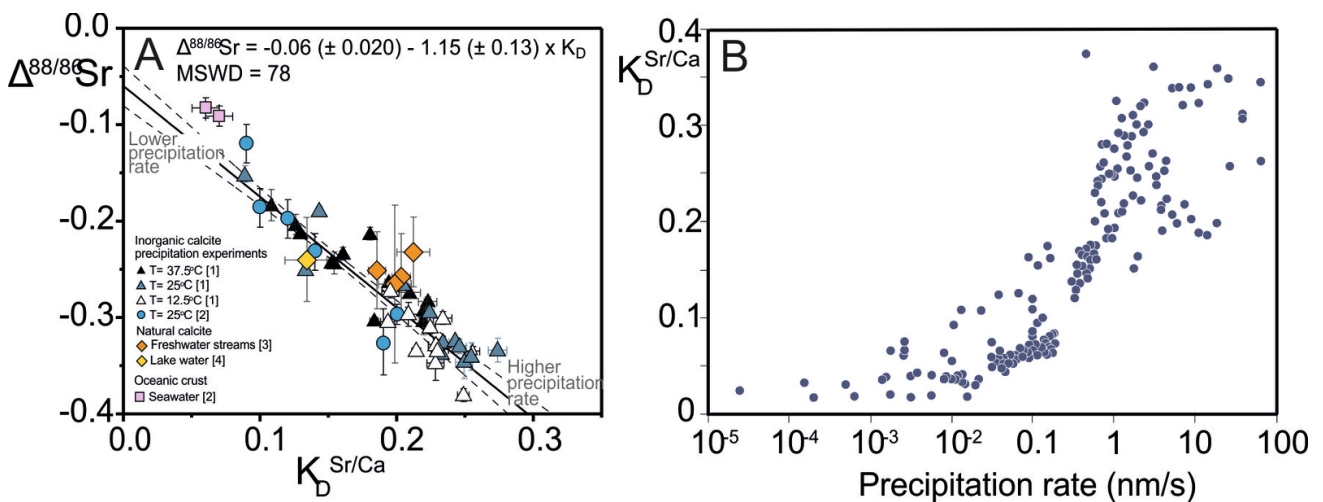
Figure 7. A) Correlation between calcite-water stable Sr isotopic fractionation factor and calcite-water Sr/Ca partition coefficient (1. AlKhatib & Eisenhauer, 2017; 2. Böhm et al., 2012; 4. Fruchter et al., 2017; 3. Shalev et al., 2017). Line and 1σ error bounds least squares fit taking into account quoted errors on both δ$^{88/86}$Sr and $K_D^{\frac{Sr}{Ca}}$ after Kent et al. (1990). B) Compilation of experimental determinations of calcite-water Sr/Ca partition coefficient compiled by Gabitov et al. (2014).

$$\frac{\partial \left(\delta^{\frac{44}{40}}Ca \cdot Ca_F \right)}{\partial x} =$$
$$R_{Ca}\, \delta^{\frac{44}{40}}Ca_{CC}$$
$$-(1+\epsilon)\, R_{Ca} \cdot \left(\delta^{\frac{44}{40}}Ca + \Delta^{\frac{44}{40}}Ca \right) \quad (3)$$

where Ca_F is given by the solution to equation (2).

The differential equation for the variation of Sr concentration in the fluid (Sr_F, nmol m^{-3}) with distance is

$$\omega_0 \phi \frac{\partial Sr_F}{\partial x} = \left. \frac{Sr}{Ca} \right|_{CC} R_{Ca}$$
$$- \frac{Sr_F}{Ca_F}\, K_D^{\frac{Sr}{Ca}}\, R_{Ca}\, (1+\epsilon) \quad (4)$$

where $K_D^{Sr/Ca}$ is the calcite-fluid Sr/Ca partition coefficient and $\left. \frac{Sr}{Ca} \right|_{CC}$ the source calcite Sr/Ca ratio. The approximate differential equation describing the mass-balance of Sr-isotopic compositions is

$$\frac{\partial \left(\delta^{88/86}Sr_F \cdot Sr_F \right)}{\partial x} =$$
$$R_{Ca}\, \delta^{88/86}Sr_{CC} \left. \frac{Sr}{Ca} \right|_{cc}$$
$$-R_{Ca}\, K_D^{Sr/Ca} \left. \frac{Sr}{Ca} \right|_{cc} \left(\delta^{88/86}Sr_F + \Delta^{88/86}Sr \right) \quad (5)$$

where Ca_F and Sr_F are given by the solutions to equations (2) and (4).

The following are convenient transformations to dimensionless variables,

$$x = h\, x'$$
$$Sr = Sr_F'\, Sr_F^0$$
$$Ca = Ca_F'\, Ca_F^0 \quad (6)$$

where h is a length scale (here flow path length) and Sr_F^0 and Ca_F^0 are the initial fluid concentrations. For given starting compositions these transformations allow the differential equations to be rewritten in terms of one variable, a Damköhler number, which defined as

$$N_D = \frac{R_{Ca}\, h}{Ca_F^0\, \omega_0\, \phi} \quad (7)$$

An alternative Damköhler number, normalised to the initial concentrations of calcite Ca in the bulk rock (N_D^{rock}), maybe used to describe the extent of rock re-crystallisation and is related to N_D by

$$N_D^{rock} = \frac{Ca_F^0}{Ca_{CC}}\, N_D \quad (8)$$

The solutions to equations (2) to (5) are given in the supplementary section S5, equations (S12) to (S21).

6.2.3. IMPLICATIONS OF THE REACTIVE TRANSPORT MODEL

The solutions for the covariation of $\delta^{88/86}$Sr values and Sr/Ca ratios for ϵ = -0.5, 0, +0.5 and ∞ (Rayleigh fractionation) for Sr-isotope and Sr/Ca fractionation factors appropriate to two precipitation rates from the correlation in figure 7A are shown in figure 8. This illustrates the major control on trajectories in $\delta^{88/86}$Sr-Sr/Ca ratio space is precipitation rate which determines the fractionation factors. Paths in which precipitation is less than dissolution (ϵ<0) are limited and go rapidly to steady state because the fluid composition is dominated by the dissolving calcite. Solu-
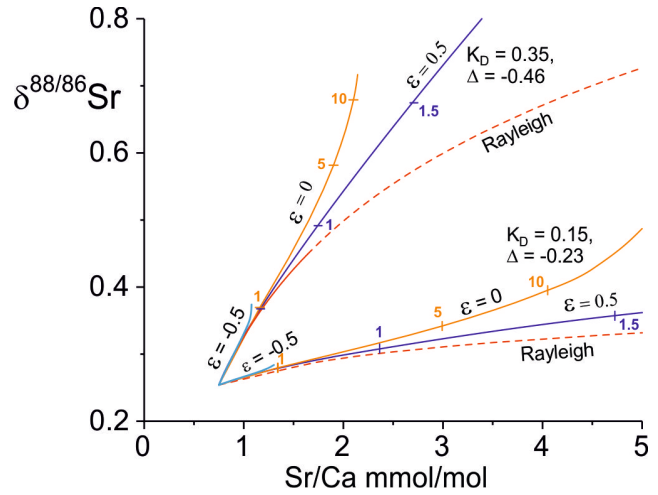
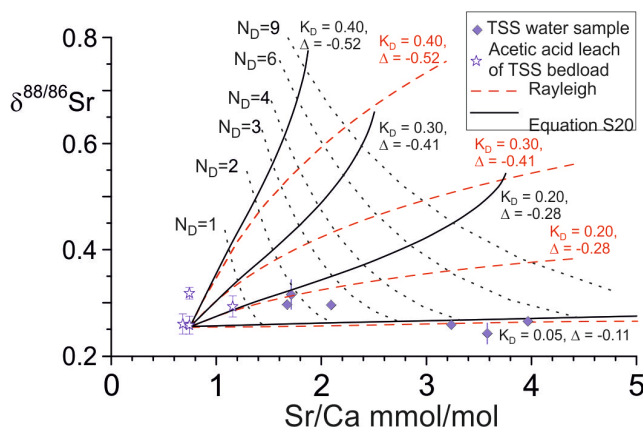**Figure 8. The evolution of $\delta^{88/86}$Sr values against Sr/Ca ratios from water with initial Sr/Ca = 0.75 and $\delta^{88/86}$Sr = 0.254‰ for values of ϵ = -0.5, 0 and 0.5 as well as by Rayleigh fractionation for values of $K_D^{\frac{Sr}{Ca}}$ and $\Delta^{88/86}$Sr shown. Damköhler numbers shown on curves. Calculated from equation (S17) and with equation (5) solved by a numerical routine. Curves for ϵ= -0.5 and 0 extend to their equilibrium Sr/Ca and $\delta^{88/86}$Sr values. For the ϵ=0.5 curves Ca goes to zero at N_D = 2.**

tions with precipitation greater than dissolution (ϵ>0) approach Rayleigh fractionation as ϵ becomes large. Natural systems will deviate from these idealized trends as fluids either become saturated in primary calcite (ϵ<0) or depleted (ϵ>0) and where the extent of reaction will be controlled by the extent of initial under- or over-saturation of calcite. In carbonate flow paths where the solution and re-precipitation of calcite is driven by the small difference in free energy between the primary Mg-calcite in the rock and the product low Mg-calcite it seems likely that re-precipitation will balance dissolution such that the Ca content of the fluid remains nearly constant. In such a system solution and re-precipitation rates will decrease slowly as fluid Mg/Ca ratios increase.

The evolution of $\delta^{88/86}$Sr values against Sr/Ca ratios for balanced solution and re-precipitation (ϵ=0) is illustrated in figure 9 as a function of the Damköhler number for a range of $K_D^{\frac{Sr}{Ca}}$ and $\Delta^{88/86}$Sr fractionation factors which co-vary as the experimentally determined precipitation-rate dependent correlation (fig. 7A). The solutions depend on the starting composition of the water, taken as the lowest bedload carbonate leach of TSS bedload, on the Sr/Ca partition coefficient and on the Damköhler number. The latter is proportional to reaction rate and flow path length and inversely proportional to the fluid flux. At low precipitation rates both $\Delta^{88/86}$Sr and $K_D^{\frac{Sr}{Ca}}$ are small and the Sr content of the fluid is dominated by the addition of Sr from the rock. The result is that there is little change in $\delta^{88/86}$Sr values, but the fluid Sr/Ca ratios increase rapidly because the secondary calcite has low Sr/Ca ratios relative to the source carbonate. At higher precipitation rates both $\Delta^{88/86}$Sr and $K_D^{\frac{Sr}{Ca}}$ are larger and the fluid $\delta^{88/86}$Sr values in-

Figure 9. The evolution of $\delta^{88/86}$Sr values against Sr/Ca ratios from water with initial Sr/Ca = 0.75 and initial $\Delta^{88/86}$Sr = 0.254‰ calculated from equations (S18) & (S20) for constant Ca in fluid (ε=0) for values of $K_D^{\frac{Sr}{Ca}}$ and $\delta^{88/86}$Sr shown (black curves which extend to equilibrium values). Damköhler number shown as dotted black contours (note that Damköhler number scales with distance along the flow path). Rayleigh fractionation curves (dashed, red) evolve to lower $\delta^{88/86}$Sr values for the equivalent Sr/Ca ratio. Data points are TSS samples from the Marsyandi and Modi Khola with 2σ internal error bars shown where larger than the symbol (table 1) and the lower ^{87}Sr/^{86}Sr acetic acid leaches of TSS bedloads (table 2).

crease more rapidly with Damköhler number (distance), but Sr/Ca ratios increase more slowly. With Rayleigh fractionation water compositions evolve to higher Sr/Ca ratios at equivalent $\delta^{88/86}$Sr values because Ca is more rapidly depleted in the fluid.

The Ca-isotopic compositions of the waters are also a function of the Ca-isotope fractionation factor, itself a function of the precipitation rate and the Damköhler number (fig. 10). However, $\delta^{44/40}$Ca values of the waters vary more rapidly with calcite solution-reprecipitation than $\delta^{88/86}$Sr values, especially at lower precipitation rates where $K_D^{\frac{Sr}{Ca}}$ is low. This is because fluid Sr isotopic compositions are buffered by the high ratio of Sr derived from mineral dissolution to that lost to secondary calcite, whereas at ε = 0, equal amounts of Ca are added to and lost from the fluid.

6.3. Interpretation of the Himalayan data

The modeling of stable Sr- and Ca-isotope analyses in conjunction with the water chemistry is used to elucidate the mechanism, magnitude and rates of formation of secondary calcites in the carbonate-dominated Marsyandi TSS catchment. The rates are compared to carbonate re-crystallisation rates inferred from catchment Ca fluxes and water-rock interactions in the Marsyandi catchment. The modeling enables comparison of the carbonate reaction rates with silicate reaction rates inferred from a similar analysis of Li isotopic compositions (Bohlin & Bickle, 2019).
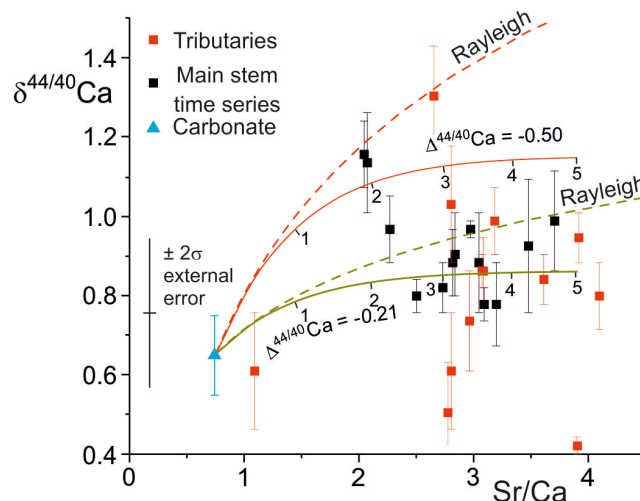
Figure 10. $\delta^{44/40}$Ca for Marsyandi TSS tributary samples and mainstem time series water samples plotted against Sr/Ca ratio (Tipper, Bickle, et al., 2006; Tipper et al., 2008; Tipper, Galy, et al., 2006, $\delta^{44/40}$Ca taken as equal to 2.1* $\delta^{44/42}$Ca). Solid curves show reactive transport trajectories calculated with balanced dissolution-re-precipitation (ε=0) with a starting composition $\delta^{44/40}$Ca = 0.65‰ (mean of three carbonate samples, Tipper, Bickle et al., 2006), Sr/Ca=0.75 and with Damköhler numbers marked. Calculated for calcite-water $\Delta^{44/40}$Ca isotopic fractionations of -0.21 and -0.50‰ and $K_D^{\frac{Sr}{Ca}}$ = 0.05. Note that if $K_D^{\frac{Sr}{Ca}}$ is increased the shape of the curves only changes slightly but the locii of the Damköhler numbers shift towards the starting point. Dashed curves show $\delta^{44/40}$Ca versus Sr/Ca ratio for Rayleigh fractionation with the same Ca-isotopic and Sr/Ca fractionation factors. Error bars 2σ internal errors on water samples and 2xstandard error on mean of three carbonate samples.

6.3.1. SR- AND CA-ISOTOPIC FRACTIONATIONS AND PRECIPITATION RATES

The TSS water samples from the Marsyandi and the Modi Khola have low Na/Ca ratios, but high Sr/Ca and Mg/Ca ratios (fig. 3) which is characteristic of carbonate-dominated catchments in which Sr/Ca and Mg/Ca ratios have been elevated by precipitation of secondary calcite. Waters in these catchments are also calcite-saturated or supersaturated (fig. 3D). The $\delta^{88/86}$Sr values show limited variation despite the high Sr/Ca ratios which have been elevated from the source limestone values by as much as a factor of 4 and plot in the region characterised with calcite precipitation rates $\leqslant 10^{-2}$ nm s^{-1} ($K_D^{\frac{Sr}{Ca}} \leqslant 0.05$, $\Delta^{88/86}$Sr $\geqslant$ -0.11‰, fig. 9). The Mg/Ca ratios exhibit similar elevations above the source limestone Mg/Ca ratios. However, their δ^{26}Mg compositions (Tipper, Galy, et al., 2006) are elevated by ~ 1‰ above bedload carbonate, consistent with the estimate of Bickle et al. (2015) that between 30 and 60% of the Mg in the waters is silicate-derived. This precludes the use of the correlation of Mg-isotope fraction factors with precipi-

tation rates (Mavromatis et al., 2013), as such shifts would swamp the ~0.1‰ Mg-isotopic fractionation factors for calcite re-precipitation.

The $\delta^{88/86}$Sr-Sr/Ca trajectories for balanced solution and re-precipitation and Rayleigh fractionation are indistinguishable at these low fractionation factors. However, as discussed in section 5.3, only a near-balanced solution-re-precipitation process is plausible as Sr concentrations increase as Ca concentrations remain approximately constant (fig. 6); also, because the low free energy difference between the Mg-calcite being dissolved and the precipitate calcite requires that the process operates with near-balanced solution and re-precipitation as discussed above. The significant addition of Mg from silicate to the waters complicates estimating Damköhler numbers from the Mg data as sites where silicate weathering products are added to the flow paths are not known. Presuming that Damköhler numbers appropriate to the Sr reactive transport apply to Mg then the secondary calcite precipitated along the flow path would have Mg/Ca ratios between ~ 0.0005 and 0.003 for the maximum likely Mg/Ca partition coefficient 0.01 (Mavromatis et al., 2013) and initial water Mg/Ca ratios of 0.046. Since the primary calcite has a Mg/Ca ratio of 0.046 (± 0.0027, 2se n=7), the mean of acetic acid leaches of bedload (Bickle et al., 2015), minimal changes in the solution-reprecipitation rate due to the increase in Mg/Ca ratios in the waters would be expected along the flow path

The $\delta^{44/40}$Ca values of the water samples analyzed by Tipper, Galy et al. (2006) (mean $\delta^{44/40}$Ca = 0.87 ± 0.04 ‰, 2se, n=20) are distinct from leaches of bedrock and bedload carbonate compositions (mean $\delta^{44/40}$Ca = 0.65 ± 0.17 ‰, 2se, n=3) (fig. 10). As for Sr, Ca concentrations and isotopic compositions would be little changed by the addition of Ca from silicates.

The correlation between stable Sr-isotope fractionation factors, $K_D^{\frac{Sr}{Ca}}$ and precipitation rates (fig. 7) implies that precipitation rates in the TSS catchments were less than ~ 10^{-2} nm/s given that $\Delta^{88/86}$Sr is equal to or less than ~ 0.1 ‰. The Ca-isotope fractionation ($\Delta^{44/42}$Ca = -0.21 ± 0.17, 2se) implies precipitation rates between 4.6×10^{-4} nm s^{-1} and 5.2×10^{-3} nm s^{-1} (2σ uncertainty on observed $\Delta^{44/42}$Ca) using the parameterisation of the experimental data compiled by Zhang and Wang (2024). However the additional uncertainty in the functional form of the relationship between Ca-isotope fractionation and precipitation rate (e.g., DePaolo, 2011; Mills et al., 2021; Z. Zhang & Wang, 2024) is rather larger than this and a realistic assessment is that the Ca-isotope data implies precipitation rates of less than ~ 5×10^{-3} nm s^{-1}.
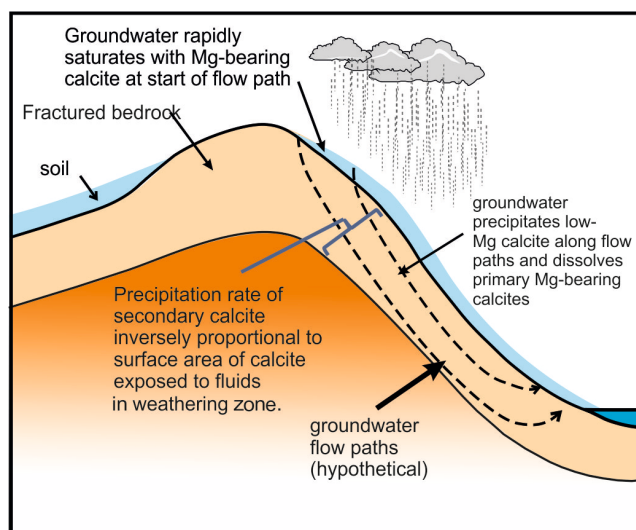
6.3.2. CALCITE RE-CRYSTALLISATION RATES COMPARED TO FIELD CONSTRAINTS

It is of interest to compare the estimated precipitation rates with calculations of the total calcite solution-precipitation rates in the catchment based on the rate of Ca exchange between fluid and minerals given by the modeling, the total flux of Ca through the catchment and the surface area of calcite crystals in contact with the fluid.

The precipitation rate of secondary calcite in the catchment may be constrained by the Damköhler number. The mean Sr/Ca of the Marsyandi time series samples collected near Chame of ~ 2.75 and their small range of $\delta^{88/86}$Sr values is consistent with an average Damköhler number of ~ 3 (range: 1.6 to 4, fig. 9), comparable with that indicated by the Ca-isotope data (fig. 10). The rate of Ca solution between water and rock along a flow path length h (m) is $R_{Ca} h$ (mol Ca s^{-1} m^{-2}). The Damköhler number (eq 5) is the ratio of the calcite solution rate along the flow path to the dissolved Ca flux. A Damköhler number of 3 therefore implies that 3 times as much Ca is dissolved, and 3 (1+ε) reprecipitated, as the dissolved Ca flux. Assuming ε = 0, the mass of calcite dissolved and re-precipitated per year is given by the water flux out of the Marsyandi TSS catchment (6.2×10^8 m^3/yr, Gabet et al., 2008) times the Ca concentration of the water (~800 µmol/L, Bickle et al., 2015) times 3, that is 1.5×10^9 mol/yr. The precipitation rate of the secondary calcite is then given by this precipitation rate divided by the surface area of the calcite in contact with the fluid in the catchment.

The calcite surface area is a function of the thickness of the weathering zone, and the surface area of exposed calcite within the weathering zone (fig. 11). We assume, as a limiting case, that all the calcite in the top 1 m of the bedrock, in the catchment area of 812 km^2, is exposed to calcite re-precipitation, that the mean fraction of calcite in the bedrock is 0.34 (fraction of calcite in the bedload sample BCT10, Bickle et al., 2015) and the mean surface area of the calcite is 0.5 m^2/g (Heling, 1968). If so, the calcite has a surface area of 4×10^{14} m^2 in the catchment. This implies a growth rate of ~5×10^{-9} nm/s, much less than the maximum rates of ~ 5×10^{-3} nm/s inferred from the calcite-water $\Delta^{44/42}$Ca fractionation with the Zhang and Wang (2024) parameterisation and also the ~10^{-2} nm/s limiting value at which $\delta^{88/86}$Sr fractionations in the solution and re-precipitation flow model appear to be sensitive to precipitation rate (fig. 7). The fraction of calcite surface area exposed to fluids in the top metre would need to be less than ~5×10^{-5} of the total calcite surface area for the re-precipitation rate to reach 10^{-4} nm/s. It is probable that groundwater circulates much deeper than 1 metre and, if so, the fraction of the area of calcite exposed to the groundwater would need to be proportionally less for re-precipitation rates to reach the critical rate of 10^{-3} nm/s. It seems very unlikely that re-precipitation rates reach values as high as 10^{-3} nm/s, unless flow takes place along widely spaced cracks.

The fraction of the calcite exported in the Marsyandi TSS catchment which is re-precipitated as low Sr- and Mg-calcite, may be calculated from the detrital flux of calcite of ~ 8×10^9 mol/yr (inferred from a total detrital flux of 2.2×10^9 kg/yr, Gabet et al., 2008, containing ~34 weight % carbonate) and the solution-reprecipitation rate of 1.5×10^9 mol Ca yr^{-1}. This fraction, at ~ 20%, is surprisingly high but addition of the re-precipitated calcite would make a negligible difference to its bulk $\delta^{88/86}$Sr values as the inferred isotopic fractionation factor is small. Integrating the precipitated calcite composition over the flow path length, the re-precipitated calcite would have a mean $\delta^{88/86}$Sr ~ 0.10 ‰ less

Figure 11. Schematic figure illustrating model for calcite recrystallisation. Rain water rapidly saturates with Mg-bearing calcites in the limestones at the start of the flow path. As the water flows along groundwater flow paths low-Mg calcite is precipitated replacing the higher Mg-calcite in the weathering zone driven by the small difference in thermodynamic stability between Mg-bearing biogenic limestone and re-precipitated low-Mg calcite. Note ground water flows are likely more complex than shown. Also thickness of soil (thin to absent), weathering zone, (possibly metres to 10's metres in fractured rock), and height above valley floor (~ 2000 m in the Marsyandi) are not to scale.

than the Mg-calcite and a mean Sr/Ca ratio of the re-precipitated calcite of ~ 0.1. Addition of this calcite would decrease the bulk $\delta^{88/86}$Sr of the detrital calcite by ~ 0.02 ‰ and its Sr/Ca ratio from 0.75 to 0.62 but these differences will be undetectable given the precision of the Sr-isotopic measurements and the heterogeneity of the bedload carbonate compositions (table 2 and data in Bickle et al., 2015). The thickness of the re-precipitated rims depends on the mean grain size. If the estimated carbonate surface area of 0.5 m^2/g was on uniform sized spherical grains, these would have a diameter of 4 μm, much less than the observed grains in the bedload, and the re-precipitated rim thickness would be ~ 0.15 μm, too thin to be easy to detect.

6.3.3. COMPARISON WITH SILICATE DISSOLUTION RATES FROM LI-ISOTOPIC COMPOSITIONS

It is of interest to compare the weathering kinetics inferred from Damköhler numbers derived from $\delta^{88/86}$Sr values with those inferred from Li-isotopic ratios since the latter reflect silicate weathering with only a minor contribution from carbonates (Kisakürek et al., 2005). The water-normalised Damköhler numbers implied by the Marsyandi $\delta^{88/86}$Sr values and Sr/Ca ratios (fig. 8) range between ~2 and 6 which translate to rock-normalised Damköhler numbers between 2×10^{-4} and 6×10^{-4}, given the average tributary water Ca concentration (~ 1 mmol/L) and the average bedload calcite

Ca concentration of 4.2 mol/kg (Bickle et al., 2015). Rock-normalised Damköhler numbers for Li dissolution in the Marsyandi TSS waters are between 3×10^{-5} to 3×10^{-4} (Bohlin & Bickle, 2019, fig. F1). The overlap in these estimates might seem surprising given that carbonate dissolution rates are generally at least an order-of-magnitude faster than silicate dissolution rates (e.g., Drever, 1997). However, the covariation of $\delta^{88/86}$Sr values and Sr/Ca ratios constrains the coupled solution-re-precipitation rate of Mg-calcites to low Mg-calcites from fluids which are presumably only slightly under-saturated with respect to Mg-calcite. These rates will be much slower than the initial dissolution by the original under-saturated rain or ground water compositions.

6.3.4. IMPLICATIONS FOR QUANTIFYING CATION INPUTS FROM SILICATE AND CARBONATE MINERALS

A key question is how the balanced solution-reprecipitation model impacts calculation of the relative proportions of silicate and carbonate inputs to the waters. The Rayleigh fractionation model assumes that the chemical weathering takes place prior to precipitation of secondary calcites as the CO_2 over-saturated waters degas and warm (e.g., Jacobson et al., 2002). If the precipitation of secondary calcite takes place along ground water flow paths, then the relative locations of the silicate and carbonate inputs and calcite solution-reprecipitation reactions will impact the resultant river chemistries. The chemical weathering processes will be governed by how the groundwater flow paths sample the different rock types in the catchment which will be controlled by the range of rock types, their geometries and physical properties. In steep rapidly eroding Himalayan catchments, groundwater flow will be through thin soils, regolith, moraines and variably fractured bedrock. River waters will represent mixtures from groundwater flow paths which may sample different combinations of carbonate rocks, silicate rocks, calc-silicate rocks, alternating carbonate and silicate rocks and variably weathered mixed regolith and moraines.

To illustrate the potential impact of balanced solution-reprecipitation on the calculation of the relative inputs of silicate and carbonate cations we explore a simple end-member model. In this the silicate-derived and carbonate-derived waters mix after passing through separate groundwater flow paths in silicate or carbonate rocks. The mass-balance equations may be written (cf. Bickle et al., 2015, equations 5 and 6)

$$X_{wat}^i = \left(E^i F_{crb.} X_{crb}^i + F_{sil} X_{sil}^i \right) \qquad (9)$$

and for ^{87}Sr/^{86}Sr

$$^{87}X$$

$$^{87}Sr/^{86}Sr_{wat}$$
$$= \frac{\left(^{87}Sr/^{86}Sr_{crb} \, F_{crb \, Sr} \, E^{Sr} \, X_{crb}^{Sr} + \, ^{87}Sr/^{86}Sr_{sil} \, F_{sil} X_{sil}^{Sr} \right)}{\left(E_{Sr} \, F_{crb} \, X_{crb}^{Sr} + \, F_{sil} X_{sil}^{Sr} \right)} \qquad (10)$$

where X_{wat}^i is the concentration of cation 'i' in the water (mmol/L), F_{crb} and F_{sil} the weight of the carbonate and silicate components (kg/L) added to the water by weathering prior to solution-reprecipitation in the carbonate groundwater flow path, X_j^i the concentration (mmol/kg) of cation

'*i*' in input phase '*j*' (carbonate or silicate) and E^i is the amount cation '*i*' is enriched by the solution-reprecipitation reactions. E^i equals 1 for Ca, Na and K since Na and K concentrations are not changed by precipitation of secondary carbonates and we model balanced solution-reprecipitation for Ca. The enrichments of Sr and Mg are functions of their respective partition coefficients and the Damköhler number (N_D) as given by equation (7). The variation of Mg calcite-water partition coefficient with precipitation rate is not well constrained with Gabitov et al. (2014) and Mavromatis et al. (2013) observing opposite relationships possibly arising from differences in fluid chemistry. However, $K_D^{Mg/Ca}$ in their experiments is constrained to lie between ~ 0.01 and 0.035 and the maximum difference between E^{Mg} and E^{Sr} is ~ +12% (at N_D = 5 and with $K_D^{Mg/Ca}$= 0.01 and $K_D^{Sr/Ca}$= 0.05). To allow for this difference the enrichment fact for Mg (E^{Mg}) has been parameterized as

$$E^{Mg} = -0.0040 + 0.9922\, E^{Sr} + 0.0127\, E^{Sr\,2} \quad (11)$$

Equations (9) and (10) have then been solved for F_{crb}, F_{sil}, X_j^i, N_D and E^{Sr} given water Sr, Ca, Mg and ^{87}Sr/^{86}Sr compositions for the Marsyandi time-series suite of samples and the silicate and carbonate compositions of the bed-load sample BCT10 (table 3). These solutions may be compared with solutions assuming calcite precipitation by Rayleigh fractionation of Bickle et al. (2015, table 2). The fractions of Sr and Mg derived from carbonate in the solution-reprecipitation model are close to those calculated from Rayleigh fractionation because in both models carbonate Sr and Mg are increased to match the observed Sr/Ca ratios and little Sr and Mg are lost to secondary calcite. However, the fraction of silicate-derived Ca delivered to the river calculated for the solution-reprecipitation process is a factor of ~ 3 higher (4.2% versus 1.3%) than calculated by Rayleigh fractionation. This difference arises because with Rayleigh fractionation the initial high Ca (both silicate and carbonate-derived) is lost to secondary calcite. With solution-reprecipitation restricted to groundwater flow paths in carbonate, silicate-derived Ca is not lost. Clearly the nature of the groundwater flow paths which control how waters interact with silicate and carbonate rocks are important controls on chemical weathering outputs and will impact the calculation of the relative inputs from silicate and carbonate sources.

The results are consistent with a major conclusion of Jacobson et al. (2002) that secondary calcite precipitation elevates Sr/Ca and Mg/Ca and precludes direct use of these ratios to estimate silicate and carbonate inputs. The modeling of balanced solution-reprecipitation in the system Sr-Ca-Mg-^{87}Sr/^{86}Sr implies water Na and K concentrations much higher than those measured (table 3) as was observed with the Rayleigh fraction model of Bickle et al. (2015). Modeling including Na, e.g., in the system Na-Sr-Ca-Mg-^{87}Sr/^{86}Sr, returns solutions with a much poorer fit (average χ^2 ~ 119 for the time series samples versus 0.6 for Sr-Ca-Mg-^{87}Sr/^{86}Sr system). A possible reason is that Na and K in rocks, from this mainly low metamorphic grade catchment, are hosted in white micas which weather slowly compared to the minerals hosting Sr, Ca and Mg. The result is that the silicate fractions of the bed load have much higher ratios of Na to Ca, Mg and Sr than the cations released to solution. This illustrates a significant uncertainty in calculating the relative inputs of silicate and carbonate minerals which is the choice of appropriate element ratios of the silicate inputs. The goodness of fit, ie. low χ^2, is a necessary indication that waters and chosen input end-member ratios lie in the appropriate hyperplane defined by the input compositions but does not require that the input phase compositions lie in their correct positions (cf. Sohn, 2013). This is a fundamental limit to the 'inversion' method for calculating carbonate and silicate inputs (e.g., Gaillardet et al., 1999; Moon et al., 2014; Négrel et al., 1993) since the inversion will yield results in which the input phase compositions lie in the mixing hyperplane defined by the water compositions but cannot determine their locations within the hyperplane.

7. CONCLUSIONS

This study shows that the $\delta^{88/86}$Sr isotopic values of carbonate in Himalayan rocks are elevated by exchange with silicate minerals as observed for ^{87}Sr/^{86}Sr ratios. Carbonate-dominated catchments (e.g., TSS) tend to exhibit lighter $\delta^{88/86}$Sr isotope compositions than those draining silicate-dominated terrains (HHCS) reflecting mass-balance between carbonate and silicate sourced Sr.

The marked increase in Sr/Ca ratios in the waters above the Sr/Ca ratio of the carbonate-dominated inputs in the TSS catchments is best modelled by balanced dissolution of bedrock Mg-calcite and re-precipitation of a low Mg-calcite. This avoids the necessity of postulating the very high initial Ca concentrations implied by simple precipitation of the secondary calcites modelled by Rayleigh fractionation and is consistent with the increase in Sr concentrations and approximately constant Ca concentrations with increasing Sr/Ca ratios in the carbonate-dominated TSS Marsyandi catchment. This conclusion is important for the calculation of silicate and carbonate chemical weathering rates in Himalayan catchments and the impact of the exhumation of the Himalayas on global climate (e.g., Kump et al., 2000). Most calculations of silicate and carbonate chemical weathering rates are based on ratios of some or all of the cations Na-K-Ca-Mg-Sr and ^{87}Sr/^{86}Sr ratios (e.g., Bickle et al., 2015; English et al., 2000; Galy & France-Lanord, 1999; Harris et al., 1998; Jacobson et al., 2002; Singh et al., 1998). The mechanism which elevates Mg/Ca and Sr/Ca ratios in the waters and its implication for magnitude of Ca inputs to the waters is critical to these calculations. The impact of solution-reprecipitation of calcites along groundwater flow paths is also dependent on how the flow paths sample silicate and carbonate rocks which adds further uncertainty to the calculations.

The limited change in $\delta^{88/86}$Sr values with increasing Sr/Ca ratios is consistent with re-precipitation of secondary calcites at low rates such that the $\delta^{88/86}$Sr fractionation factor and Sr/Ca partition coefficient are both small. These rates are consistent with field estimates of the rate of calcite re-crystallisation based on the flux of dissolved Ca out of the Marsyandi catchment, the amount of Ca exchanged

Table 3. **Comparison of Rayleigh fractionation and balanced dissolution-reprecipitation models for calculation of silicate and carbonate inputs to Marsyandi time-series samples. Cation concentrations of waters** μ**mol/L except Sr nmol/L.**

Elements in regression	χ^2 mean	E_{Sr} 1σ	Fsill 1σ	Fcrb 1σ	Sr	Ca	Mg	Na	K	^{87}Sr/^{86}Sr	**%Ca$_{sill}$ 1σ	%Sr$_{sill}$ 1σ	%Mg$_{sill}$ 1σ	N$_D$ *** max min
Water*					2372	851	433	86	27	0.71709				
Rayleigh*	0.4	3.4 0.5	1.93 0.14	0.9 0.06	2358	850	432	411	637	0.71759	1.3 0.4	22.8 2.0	61.0 2.7	
Balanced	0.6	3.5 0.5	1.76 0.69	0.24 0.03	2336	851	436	373	578	0.71751	4.2 1.4	22.3 5.1	58.8 7.6	4.1 1.8

Averages of results of regressing individual Marsyandi time-series suite of water samples corrected for cyclic inputs (Tipper, Bickle, et al., 2006, table 2, excluding sample MT25) against BCT10 acetic leach plus silicate-corrected HCl leach for carbonate component and BCT10 residue for Sr-Ca-Mg-^{87}Sr/^{86}Sr. E^{Sr} for Rayleigh fractionation calculated as γ$^{(KdSr-1)}$, the increase in Sr/Ca ratio to be comparable to E^{Sr} calculated for the balanced dissolution-reprecipitation model. Uncertainty estimates 1σ. Numerical solution of equations as Bickle et al. (2015).

Rayleigh: Silicate and carbonate components added prior to precipitation of secondary calcite by Rayleigh fractionation after Bickle et al. (2015, table 2 top row).

Balanced: Assumes silicate and carbonate components added after balanced solution-reprecipitation reactions in the carbonate groundwater flow path.

* Water compositions are average of time-series samples corrected for saline inputs given by Bickle et al. (2015, table 2 top row).

** Percentage of silicate cations calculated after groundwater flow paths -i.e. assumed output to river.

*** Range of Damköhler Numbers (N$_D$) calculated from enrichment factor for Sr (E^{Sr}) from equation S17 (supplementary information).

by solution-re-precipitation and the likely surface area of calcite in the weathering zone. The low $\Delta^{88/86}$Sr isotopic fractionation factors are also consistent with previously inferred $\Delta^{44/42}$Ca calcite water fractionation factors (e.g., Z. Zhang & Wang, 2024). However, if these go to zero as calcite-water equilibrium is approached, the calcite re-precipitation rates imply that only a small fraction of the surface area of calcite in the weathering zone is recrystallising at any one time.

The calcite-re-precipitation rates are of the same order-of-magnitude as the rates of silicate mineral dissolution previously inferred from Li isotopic compositions (Bohlin & Bickle, 2019). These carbonate precipitation rates are presumed to be low because the solution-re-precipitation reactions take place at close to equilibrium which must contrast with the initial dissolution of calcite which rapidly raises calcite saturation in the groundwaters.

This data set adds to the growing database of riverine $\delta^{88/86}$Sr calcite water fractionation factors and the utility of $\delta^{88/86}$Sr, especially with regards to combining $\delta^{88/86}$Sr with other non-traditional isotope systems (e.g., δ^7Li, δ^{30}Si and δ^{26}Mg). Assessing characteristic Damköhler numbers for these isotope systems offers a rapid method for comparing reaction rates but more needs to be known about the reaction stoichiometries controlling the isotopic fractionations and on groundwater flow paths and mixing in catchments to be able to properly interpret the data.

<center>,,,</center>

Author contributions

Emily Stevenson carried out the stable Sr-isotope and most of the geochemical analyses, wrote the first draft of the paper and led the various revisions. Kevin Burton and Ian Parkinson conceptualised and funded the research, supervising the writing of the manuscript and laboratory analysis. Rachael James and Basak Kisakürek collected most of the samples and supplied unpublished geochemical data on the samples, Ed Tipper & Emily Stevenson developed analytical methods for $\delta^{88/86}$Sr at Cambridge, Mike Bickle developed the solution-precipitation model and derived the analytical solutions for the reactive transport modeling. All authors contributed to revising the many drafts of the manuscript.

Supplementary Information

https://doi.org/10.5285/ad233bd1-9e07-4729-bb3e-776e09a02a3a

Editor: C. Page Chamberlain, Associate Editor: Mark Albert Torres

REFERENCES

Ahmad, T., Harris, N., Bickle, M., Chapman, H., Bunbury, J., & Prince, C. (2000). Isotopic constraints on the structural relationships between the Lesser Himalayan Series and the High Himalayan Crystalline Series, Garhwal Himalaya. *GSA Bulletin*, *112*(3), 467–477. https://doi.org/10.1130/0016-7606(2000)112

Albarède, F., & Beard, B. (2004). Analytical methods for non-traditional isotopes. *Geochemistry of Non-Traditional Stable Isotopes. Reviews in Mineralogy & Geochemistry*, *55*, 113–152. https://doi.org/10.2138/gsrmg.55.1.113

AlKhatib, M., & Eisenhauer, A. (2017). Calcium and strontium isotope fractionation in aqueous solutions as a function of temperature and reaction rate; I. Calcite. *Geochimica et Cosmochimica Acta*, *209*, 296–319. https://doi.org/10.1016/j.gca.2016.09.035

Andrews, M. G., & Jacobson, A. D. (2018). Controls on the solute geochemistry of subglacial discharge from the Russell Glacier, Greenland Ice Sheet determined by radiogenic and stable Sr isotope ratios. *Geochimica et Cosmochimica Acta*, *239*, 312–329. https://doi.org/10.1016/j.gca.2018.08.004

Andrews, M. G., Jacobson, A. D., Lehn, G. O., Horton, T. W., & Craw, D. (2016). Radiogenic and stable Sr isotope ratios (^{87}Sr/^{86}Sr, $\delta^{88/86}$Sr) as tracers of riverine cation sources and biogeochemical cycling in the Milford Sound region of Fiordland, New Zealand. *Geochimica et Cosmochimica Acta*, *173*, 284–303. https://doi.org/10.1016/j.gca.2015.10.005

Becker, J. A. (2005). *Quantification of Himalayan Metamorphic CO2 Fluxes. Impact on Global Carbon Budgets* [PhD]. University of Cambridge.

Becker, J. A., Bickle, M. J., Galy, A., & Holland, T. J. B. (2008). Himalayan metamorphic CO_2 fluxes: quantitative constraints from hydrothermal springs. *Earth and Planetary Science Letters*, *265*(3–4), 616–629. https://doi.org/10.1016/j.epsl.2007.10.046

Berner, R. A., Lasaga, A. C., & Garrels, R. M. (1983). The carbonate-silicate geochemical cycle and its effect on atmospheric carbon dioxide over the past 100 million years. *American Journal of Science*, *283*(7), 641–683. https://doi.org/10.2475/ajs.283.7.641

Bickle, M. J., Harris, N. B. W., Bunbury, J. M., Chapman, H. J., Fairchild, I. J., & Ahmad, T. (2001). Controls on the ^{87}Sr/^{86}Sr Ratio of Carbonates in the Garhwal Himalaya, Headwaters of the Ganges. *The Journal of Geology*, *109*(6), 737–753. https://doi.org/10.1086/323192

Bickle, M. J., Tipper, E., Galy, A., Chapman, H., & Harris, N. (2015). On discrimination between carbonate and silicate inputs to Himalayan rivers. *American Journal of Science*, *315*(2), 120–166. https://doi.org/10.2475/02.2015.02

Bohlin, M. S., & Bickle, M. J. (2019). The reactive transport of Li as a monitor of weathering processes in kinetically limited weathering regimes. *Earth and Planetary Science Letters*, *511*, 233–243. https://doi.org/10.1016/j.epsl.2019.01.034

Böhm, F., Eisenhauer, A., Tang, J., Dietzel, M., Krabbenhöft, A., Kisakürek, B., & Horn, C. (2012). Strontium isotope fractionation of planktic foraminifera and inorganic calcite. *Geochimica et Cosmochimica Acta*, *93*, 300–314. https://doi.org/10.1016/j.gca.2012.04.038

Bordet, P., Colchen, M., Krummenacher, D., Le Fort, P., Mouterde, R., & Remy, M. (1971). *Recherches Geologiques dans l'Himalaya du Nepal, Region de la Thakkhola* (Vol. 86). Centre National de la recherche Scientifique.

Bordet, P., Colchen, M., & Le Fort, P. (1975). *Recherches géologiques dans l'Himalaya du Népal, région du Nyi-Shang*. Centre National de la Recherche Scientifique.

Bouchez, J., & von Blanckenburg, F. (2021). The role of vegetation in setting strontium stable isotope ratios in the Critical Zone. *American Journal of Science*, *321*(8), 1246–1283. https://doi.org/10.2475/08.2021.04

Bullen, T., & Chadwick, O. (2016). Ca, Sr and Ba stable isotopes reveal the fate of soil nutrients along a tropical climosequence in Hawaii. *Chemical Geology*, *422*, 25–45. https://doi.org/10.1016/j.chemgeo.2015.12.008

Burbank, D. W., Blythe, A. E., Putkonen, J., Pratt-Sitaula, B., Gabet, E., Oskin, M., Barros, A., & Ojha, T. P. (2003). Decoupling of erosion and precipitation in the Himalayas. *Nature*, *426*(6967), 652–655. https://doi.org/10.1038/nature02187

Calmels, D. (2007). *Alteration chimique des carbonates: Influence des sources d'acidité sur les bilans globaux* [PhD Thesis]. Universite Paris 7–Denis Diderot.

Chamberlin, T. C. (1898). The influence of great epochs of limestone formation upon the constitution of the atmosphere. *The Journal of Geology*, *6*(6), 609–621. https://doi.org/10.1086/608185

Chao, H.-C., You, C.-F., Liu, H.-C., & Chung, C.-H. (2015). Evidence for stable Sr isotope fractionation by silicate weathering in a small sedimentary watershed in southwestern Taiwan. *Geochimica et Cosmochimica Acta*, *165*, 324–341. https://doi.org/10.1016/j.gca.2015.06.006

Chen, B.-B., Li, S.-L., Pogge von Strandmann, P. A. E., Wilson, D. J., Zhong, J., Sun, J., & Liu, C.-Q. (2022). Calcium isotopes tracing secondary mineral formation in the high-relief Yalong River Basin, Southeast Tibetan Plateau. *Science of The Total Environment*, *827*, 154315. https://doi.org/10.1016/j.scitotenv.2022.154315

Coogan, L. A., & Dosso, S. E. (2015). Alteration of ocean crust provides a strong temperature dependent feedback on the geological carbon cycle and is a primary driver of the Sr-isotopic composition of seawater. *Earth and Planetary Science Letters*, *415*, 38–46. https://doi.org/10.1016/j.epsl.2015.01.027

de Souza, G. F., Reynolds, B. C., Kiczka, M., & Bourdon, B. (2010). Evidence for mass-dependent isotopic fractionation of strontium in a glaciated granitic watershed. *Geochimica et Cosmochimica Acta*, *74*(9), 2596–2614. https://doi.org/10.1016/j.gca.2010.02.012

DePaolo, D. J. (2011). Surface kinetic model for isotopic and trace element fractionation during precipitation of calcite from aqueous solutions. *Geochimica et Cosmochimica Acta*, *75*(4), 1039–1056. https://doi.org/10.1016/j.gca.2010.11.020

Drever, J. I. (1997). *The geochemistry of natural waters: Surface and Groundwater Enviromnments*. Prentice Hall.

Duvadi, A. K., Pradhan, P. M., Shrestha, O. M., Dhoubhadel, T. P., Piya, P., & Chand, J. B. (2005). *Geological map of parts of Sindhupalchok and Nuwakot districts (Melamchi area). Sheet No. 2785 03 (72E/9)*. Department of Mines and Geology, Kathmandu, Nepal.

Edmond, J. M. (1992). Himalayan tectonics, weathering processes, and the strontium isotope record in marine limestones. *Science*, *258*(5088), 1594–1597. https://doi.org/10.1126/science.258.5088.1594

English, N. B., Quade, J., DeCelles, P. G., & Garzione, C. N. (2000). Geologic control of Sr and major element chemistry in Himalayan Rivers, Nepal. *Geochimica et Cosmochimica Acta*, *64*(15), 2549–2566. https://doi.org/10.1016/s0016-7037(00)00379-3

Evans, M. J., Derry, L. A., & France-Lanord, C. (2004). Geothermal fluxes of alkalinity in the Narayani river system of central Nepal. *Geochemistry, Geophysics, Geosystems*, *5*(8). https://doi.org/10.1029/2004gc000719

Fietzke, J., & Eisenhauer, A. (2006). Determination of temperature-dependent stable strontium isotope (^{88}Sr/^{86}Sr) fractionation via bracketing standard MC-ICP-MS. *Geochemistry, Geophysics, Geosystems*, *7*(8). https://doi.org/10.1029/2006gc001243

Fontorbe, G., De La Rocha, C. L., Chapman, H. J., & Bickle, M. J. (2013). The silicon isotopic composition of the Ganges and its tributaries. *Earth and Planetary Science Letters*, *381*, 21–30. https://doi.org/10.1016/j.epsl.2013.08.02

Fruchter, N., Lazar, B., Nishri, A., Almogi-Labin, A., Eisenhauer, A., Be'eri Shlevin, Y., & Stein, M. (2017). ^{88}Sr/^{86}Sr fractionation and calcite accumulation rate in the Sea of Galilee. *Geochimica et Cosmochimica Acta*, *215*, 17–32. https://doi.org/10.1016/j.gca.2017.07.026

Gabet, E. J., Burbank, D. W., Pratt-Sitaula, B., Putkonen, J., & Bookhagen, B. (2008). Modern erosion rates in the High Himalayas of Nepal. *Earth and Planetary Science Letters*, *267*(3–4), 482–494. https://doi.org/10.1016/j.epsl.2007.11.059

Gabitov, R. I., Sadekov, A., & Leinweber, A. (2014). Crystal growth rate effect on Mg/Ca and Sr/Ca partitioning between calcite and fluid: An in situ approach. *Chemical Geology*, *367*, 70–82. https://doi.org/10.1016/j.chemgeo.2013.12.019

Gaillardet, J., Calmels, D., Romero-Mujalli, G., Zakharova, E., & Hartmann, J. (2019). Global climate control on carbonate weathering intensity. *Chemical Geology*, *527*, 118762. https://doi.org/10.1016/j.chemgeo.2018.05.009

Gaillardet, J., Dupré, B., Louvat, P., & Allègre, C. J. (1999). Global silicate weathering and CO_2 consumption rates deduced from the chemistry of large rivers. *Chemical Geology*, *159*(1–4), 3–30. https://doi.org/10.1016/s0009-2541(99)00031-5

Galy, A., & France-Lanord, C. (1999). Weathering processes in the Ganges-Brahmaputra basin and the riverine alkalinity budget. *Chemical Geology*, *159*(1–4), 31–60. https://doi.org/10.1016/s0009-2541(99)00033-9

Galy, A., France-Lanord, C., & Derry, L. A. (1999). The strontium isotopic budget of Himalayan Rivers in Nepal and Bangladesh. *Geochimica et Cosmochimica Acta*, *63*(13–14), 1905–1925. https://doi.org/10.1016/s0016-7037(99)00081-2

Gieskes, J. M., Kastner, M., & Warner, T. B. (1975). Evidence for extensive diagenesis, Madagascar Basin, Deep Sea Drilling Site 245. *Geochimica et Cosmochimica Acta*, *39*(10), 1385–1393. https://doi.org/10.1016/0016-7037(75)90117-9

Godard, V., Burbank, D. W., Bourlès, D. L., Bookhagen, B., Braucher, R., & Fisher, G. B. (2012). Impact of glacial erosion on ^{10}Be concentrations in fluvial sediments of the Marsyandi catchment, central Nepal. *Journal of Geophysical Research: Earth Surface*, *117*(F3). https://doi.org/10.1029/2011jf002230

Harris, N., Bickle, M., Chapman, H., Fairchild, I., & Bunbury, J. (1998). The significance of Himalayan rivers for silicate weathering rates: evidence from the Bhote Kosi tributary. *Chemical Geology*, *144*(3–4), 205–220. https://doi.org/10.1016/s0009-2541(97)00132-0

Heling, D. (1968). Microporosity of carbonate rocks. In G. Muller & G. M. Friedman (Eds.), *Recent developments in carbonate sedimentology in Central Europe* (pp. 98–105). Springer. https://doi.org/10.1007/978-3-642-88052-0_12

Jacobson, A. D., Blum, J. D., & Walter, L. M. (2002). Reconciling the elemental and Sr isotope composition of Himalayan weathering fluxes: Insights from the carbonate geochemistry of stream waters. *Geochimica et Cosmochimica Acta*, *66*(19), 3417–3429. https://doi.org/10.1016/s0016-7037(02)00951-1

Kent, J. T., Watson, G. S., & Onstott, T. C. (1990). Fitting straight lines and planes with an application to radiometric dating. *Earth and Planetary Science Letters*, *97*(1–2), 1–17. https://doi.org/10.1016/0012-821x(90)90094-e

Kisakürek, B., James, R. H., & Harris, N. B. W. (2005). Li and δ^7Li in Himalayan rivers: Proxies for silicate weathering? *Earth and Planetary Science Letters*, *237*(3–4), 387–401. https://doi.org/10.1016/j.epsl.2005.07.019

Klaver, M., Lewis, J., Parkinson, I. J., Elburg, M. A., Vroon, P. Z., Kelley, K. A., & Elliott, T. (2020). Sr isotopes in arcs revisited: tracking slab dehydration using $\delta^{88/86}$Sr and ^{87}Sr/^{86}Sr systematics of arc lavas. *Geochimica et Cosmochimica Acta*, *288*, 101–119. https://doi.org/10.1016/j.gca.2020.08.010

Krabbenhöft, A., Eisenhauer, A., Böhm, F., Vollstaedt, H., Fietzke, J., Liebetrau, V., Augustin, N., Peucker-Ehrenbrink, B., Müller, M. N., Horn, C., Hansen, B. T., Nolte, N., & Wallmann, K. (2010). Constraining the marine strontium budget with natural strontium isotope fractionations (^{87}Sr/^{86}Sr∗, $\delta^{88/86}$Sr) of carbonates, hydrothermal solutions and river waters. *Geochimica et Cosmochimica Acta*, *74*(14), 4097–4109. https://doi.org/10.1016/j.gca.2010.04.009

Krishnaswami, S., & Singh, S. K. (1998). Silicate and carbonate weathering in the drainage basins of the Ganga-Ghaghara-Indus head waters: contributions to major ion and Sr isotope geochemistry. *Proceedings of the Indian Academy of Sciences - Earth and Planetary Sciences*, *107*, 283–291. https://doi.org/10.1007/bf02841595

Kump, L. R., Brantley, S. L., & Arthur, M. A. (2000). Chemical, Weathering, Atmospheric CO_2, and Climate. *Annual Review of Earth and Planetary Sciences*, *28*(1), 611–667. https://doi.org/10.1146/annurev.earth.28.1.611

Le Fort, P. (1975). Himalayas: The collided range: Present knowledge of the continental arc. *American Journal of Science*, *275A*, 1–44.

Li, S., Li, G. K., Li, W., Chen, Y., Raymo, M. E., & Chen, J. (2023). Effects of Secondary Carbonate Precipitation and Dissolution on Changjiang (Yangtze) River Chemistry and Estimates of Silicate Weathering Rates. *Global Biogeochemical Cycles*, *37*(5). https://doi.org/10.1029/2022gb007581

Lichtner, P. C. (1988). The quasi-stationary state approximation to coupled mass transport and fluid-rock interaction in a porous medium. *Geochimica et Cosmochimica Acta*, *52*(1), 143–165. https://doi.org/10.1016/0016-7037(88)90063-4

Ma, J., Wei, G., Liu, Y., Ren, Z., Xu, Y., & Yang, Y. (2013). Precise measurement of stable ($\delta^{88/86}$Sr) and radiogenic (^{87}Sr/^{86}Sr) strontium isotope ratios in geological standard reference materials using MC-ICP-MS. *Chinese Science Bulletin*, *58*(25), 3111–3118. https://doi.org/10.1007/s11434-013-5803-5

Maher, K. (2010). The dependence of chemical weathering rates on fluid residence time. *Earth and Planetary Science Letters*, *294*(1–2), 101–110. https://doi.org/10.1016/j.epsl.2010.03.010

Mavromatis, V., Gautier, Q., Bosc, O., & Schott, J. (2013). Kinetics of Mg partition and Mg stable isotope fractionation during its incorporation in calcite. *Geochimica et Cosmochimica Acta*, *114*, 188–203. https://doi.org/10.1016/j.gca.2013.03.024

Mills, J. V., DePaolo, D. J., & Lammers, L. N. (2021). The influence of Ca:CO$_3$ stoichiometry on Ca isotope fractionation: Implications for process-based models of calcite growth. *Geochimica et Cosmochimica Acta*, *298*, 87–111. https://doi.org/10.1016/j.gca.2021.01.016

Moon, S., Chamberlain, C. P., & Hilley, G. E. (2014). New estimates of silicate weathering rates and their uncertainties in global rivers. *Geochimica et Cosmochimica Acta*, *134*, 257–274. https://doi.org/10.1016/j.gca.2014.02.033

Moynier, F., Agranier, A., Hezel, D. C., & Bouvier, A. (2010). Sr stable isotope composition of Earth, the Moon, Mars, Vesta and meteorites. *Earth and Planetary Science Letters*, *300*(3–4), 359–366. https://doi.org/10.1016/j.epsl.2010.10.017

Négrel, P., Allègre, C. J., Dupré, B., & Lewin, E. (1993). Erosion sources determined by inversion of major and trace element ratios and strontium isotopic ratios in river water: The Congo Basin case. *Earth and Planetary Science Letters*, *120*(1–2), 59–76. https://doi.org/10.1016/0012-821x(93)90023-3

Niemi, N. A., Oskin, M., Burbank, D. W., Heimsath, A. M., & Gabet, E. J. (2005). Effects of bedrock landslides on cosmogenically determined erosion rates. *Earth and Planetary Science Letters*, *237*(3–4), 480–498. https://doi.org/10.1016/j.epsl.2005.07.009

Oliver, L., Harris, N., Bickle, M., Chapman, H., Dise, N., & Horstwood, M. (2003). Silicate weathering rates decoupled from the ^{87}Sr/^{86}Sr ratio of the dissolved load during Himalayan erosion. *Chemical Geology*, *201*(1–2), 119–139. https://doi.org/10.1016/s0009-2541(03)00236-5

Palmer, M. R., & Edmond, J. M. (1992). Controls over the strontium isotope composition of river water. *Geochimica et Cosmochimica Acta*, *56*(5), 2099–2111. https://doi.org/10.1016/0016-7037(92)90332-d

Parsons, A. J., Law, R. D., Searle, M. P., Phillips, R. J., & Lloyd, G. E. (2016). Geology of the Dhaulagiri-Annapurna-Manaslu Himalaya, Western Region, Nepal. 1:200,000. *Journal of Maps*, *12*(1), 100–110. https://doi.org/10.1080/17445647.2014.984784

Pearce, C. R., Parkinson, I. J., Gaillardet, J., Charlier, B. L. A., Mokadem, F., & Burton, K. W. (2015). Reassessing the stable ($\delta^{88/86}$Sr) and radiogenic (^{87}Sr/^{86}Sr) strontium isotopic composition of marine inputs. *Geochimica et Cosmochimica Acta*, *157*, 125–146. https://doi.org/10.1016/j.gca.2015.02.029

Quade, J., Roe, L., DeCelles, P. G., & Ojha, T. P. (1997). The Late Neogene ^{87}Sr/^{86}Sr record of lowland Himalayan rivers. *Science*, *276*(5320), 1828–1831. https://doi.org/10.1126/science.276.5320.1828

Richter, F. M., & DePaolo, D. J. (1987). Numerical models for diagenesis and the Neogene Sr isotopic evolution of seawater from DSDP Site 590B. *Earth and Planetary Science Letters*, *83*(1–4), 27–38. https://doi.org/10.1016/0012-821x(87)90048-3

Richter, F. M., Rowley, D. B., & DePaolo, D. J. (1992). Sr isotope evolution of seawater: the role of tectonics. *Earth and Planetary Science Letters*, *109*(1–2), 11–23. https://doi.org/10.1016/0012-821x(92)90070-c

Ruddiman, W. F. (1997). *Tectonic uplift and climate change*. Plenum. https://doi.org/10.1007/978-1-4615-5935-1

Schneider, C., & Masch, L. (1993). The metamorphism of the Tibetan Series from the Manang area, Marsyandi Valley, central Nepal. *Geological Society, London, Special Publications*, *74*(1), 357–374. https://doi.org/10.1144/gsl.sp.1993.074.01.24

Searle, M. P., & Godin, L. (2003). The South Tibetan Detachment and the Manaslu Leucogranite: A Structural Reinterpretation and Restoration of the Annapurna-Manaslu Himalaya, Nepal. *The Journal of Geology*, *111*(5), 505–523. https://doi.org/10.1086/376763

Shalev, N., Gavrieli, I., Halicz, L., Sandler, A., Stein, M., & Lazar, B. (2017). Enrichment of ^{88}Sr in continental waters due to calcium carbonate precipitation. *Earth and Planetary Science Letters*, *459*, 381–393. https://doi.org/10.1016/j.epsl.2016.11.042

Singh, S. K., Trivedi, J. R., Pande, K., Ramesh, R., & Krishnaswami, S. (1998). Chemical and strontium, oxygen, and carbon isotopic compositions of carbonates from the Lesser Himalaya: Implications to the strontium isotope composition of the source waters of the Ganga, Ghaghara, and the Indus rivers. *Geochimica et Cosmochimica Acta*, *62*(5), 743–755. https://doi.org/10.1016/s0016-7037(97)00381-5

Sleep, N. H., & Zahnle, K. (2001). Carbon dioxide cycling and implications for climate on ancient Earth. *Journal of Geophysical Research: Planets*, *106*(E1), 1373–1399. https://doi.org/10.1029/2000je001247

Sohn, R. A. (2013). A method for inverting ratio-ratio data to estimate end-member compositions in mixing problems. *Chemical Geology*, *352*, 63–69. https://doi.org/10.1016/j.chemgeo.2013.06.002

Stevenson, E. I., Aciego, S. M., Chutcharavan, P., Parkinson, I. J., Burton, K. W., Blakowski, M. A., & Arendt, C. A. (2016). Insights into combined radiogenic and stable strontium isotopes as tracers for weathering processes in subglacial environments. *Chemical Geology*, *429*, 33–43. https://doi.org/10.1016/j.chemgeo.2016.03.008

Stevenson, E. I., Hermoso, M., Rickaby, R. E. M., Tyler, J. J., Minoletti, F., Parkinson, I. J., Mokadem, F., & Burton, K. W. (2014). Controls on stable strontium isotope fractionation in coccolithophores with implications for the marine Sr cycle. *Geochimica et Cosmochimica Acta*, *128*, 225–235. https://doi.org/10.1016/j.gca.2013.11.043

Tipper, E. T., Bickle, M. J., Galy, A., West, A. J., Pomiès, C., & Chapman, H. J. (2006). The short term climatic sensitivity of carbonate and silicate weathering fluxes: Insight from seasonal variations in river chemistry. *Geochimica et Cosmochimica Acta*, *70*(11), 2737–2754. https://doi.org/10.1016/j.gca.2006.03.005

Tipper, E. T., Galy, A., & Bickle, M. J. (2006). Riverine evidence for a fractionated reservoir of Ca and Mg on the continents: Implications for the oceanic Ca cycle. *Earth and Planetary Science Letters*, *247*(3–4), 267–279. https://doi.org/10.1016/j.epsl.2006.04.033

Tipper, E. T., Galy, A., & Bickle, M. J. (2008). Calcium and Magnesium isotope systematics in rivers draining the Himalaya-Tibetan-Plateau region: Lithological or fractionation control? *Geochimica et Cosmochimica Acta*, *72*(4), 1057–1075. https://doi.org/10.1016/j.gca.2007.11.029

Torres, M. A., West, A. J., & Li, G. (2014). Sulphide oxidation and carbonate dissolution as a source of CO_2 over geological timescales. *Nature*, *507*(7492), 346–349. https://doi.org/10.1038/nature13030

Vance, D., Bickle, M., Ivy-Ochs, S., & Kubik, P. W. (2003). Erosion and exhumation in the Himalaya from cosmogenic isotope inventories of river sediments. *Earth and Planetary Science Letters*, *206*(3–4), 273–288. https://doi.org/10.1016/s0012-821x(02)01102-0

Voigt, J., Hathorne, E. C., Frank, M., Vollstaedt, H., & Eisenhauer, A. (2015). Variability of carbonate diagenesis in equatorial Pacific sediments deduced from radiogenic and stable Sr isotopes. *Geochimica et Cosmochimica Acta*, *148*, 360–377. https://doi.org/10.1016/j.gca.2014.10.001

Walker, J. C. G., Hays, P. B., & Kasting, J. F. (1981). A negative feedback mechanism for the long-term stabilization of Earth's surface temperature. *Journal of Geophysical Research: Oceans*, *86*(C10), 9776–9782. https://doi.org/10.1029/jc086ic10p09776

Wei, G., Ma, J., Liu, Y., Xie, L., Lu, W., Deng, W., Ren, Z., Zeng, T., & Yang, Y. (2013). Seasonal changes in the radiogenic and stable strontium isotopic composition of Xijiang River water: Implications for chemical weathering. *Chemical Geology*, *343*, 67–75. https://doi.org/10.1016/j.chemgeo.2013.02.004

Weis, D., Kieffer, B., Maerschalk, C., Barling, J., de Jong, J., Williams, G. A., Hanano, D., Pretorius, W., Mattielli, N., Scoates, J. S., Goolaerts, A., Friedman, R. M., & Mahoney, J. B. (2006). High-precision isotopic characterization of USGS reference materials by TIMS and MC-ICP-MS. *Geochemistry, Geophysics, Geosystems*, *7*(8). https://doi.org/10.1029/2006gc001283

West, A. J., Arnold, M., AumaÎtre, G., Bourlès, D. L., Keddadouche, K., Bickle, M., & Ojha, T. (2015). High natural erosion rates are the backdrop for present-day soil erosion in the agricultural Middle Hills of Nepal. *Earth Surface Dynamics*, *3*(3), 363–387. https://doi.org/10.5194/esurf-3-363-2015

Wu, N., Zhang, J., Mao, H., Zhang, G., & Zhao, Z. (2024). Geochemical behavior of stable strontium isotopes during continental weathering process: A review. *Geosystems and Geoenvironment*, *3*(2), 100144. https://doi.org/10.1016/j.geogeo.2022.100144

Xu, J., Yang, S., Yang, Y., Liu, Y., & Xie, X. (2020). Precise Determination of Stable Strontium Isotopic Compositions by MC-ICP-MS. *Atomic Spectroscopy*, *41*(2), 64–73. https://doi.org/10.46770/as.2020.02.003

Zhang, S., & DePaolo, D. J. (2021). Equilibrium calcite-fluid Sr/Ca partition coefficient from marine sediment and pore fluids. *Geochimica et Cosmochimica Acta*, *289*, 33–46. https://doi.org/10.1016/j.gca.2020.08.017

Zhang, Z., & Wang, J. (2024). Quantification of classical and non-classical crystallization pathways in calcite precipitation. *Earth and Planetary Science Letters*, *636*, 118712. https://doi.org/10.1016/j.epsl.2024.118712

SUPPLEMENTARY MATERIALS

README

Download: https://ajsonline.org/article/124202-calcite-dissolution-reprecipitation-reactions-are-a-key-control-on-the-sr-ca-mg-ca-and-delta-88-86-sr-compositions-of-himalayan-river-waters/attachment/249203.txt

Supplementary information

Download: https://ajsonline.org/article/124202-calcite-dissolution-reprecipitation-reactions-are-a-key-control-on-the-sr-ca-mg-ca-and-delta-88-86-sr-compositions-of-himalayan-river-waters/attachment/249204.pdf

Supplementary Table1

Download: https://ajsonline.org/article/124202-calcite-dissolution-reprecipitation-reactions-are-a-key-control-on-the-sr-ca-mg-ca-and-delta-88-86-sr-compositions-of-himalayan-river-waters/attachment/249205.csv

Supplementary Table2

Download: https://ajsonline.org/article/124202-calcite-dissolution-reprecipitation-reactions-are-a-key-control-on-the-sr-ca-mg-ca-and-delta-88-86-sr-compositions-of-himalayan-river-waters/attachment/249206.csv

Supplementary Table3

Download: https://ajsonline.org/article/124202-calcite-dissolution-reprecipitation-reactions-are-a-key-control-on-the-sr-ca-mg-ca-and-delta-88-86-sr-compositions-of-himalayan-river-waters/attachment/249207.csv